

Spontaneous and Evoked Periodic Activity in
the Larval Zebrafish Telencephalon

MILLER ANDREW STEVEN

Doctor of Philosophy

Department of Genetics

School of Life Science

SOKENDAI (The Graduate University for
Advanced Studies)

**Spontaneous and Evoked Periodic Activity
in the Larval Zebrafish Telencephalon**

Doctoral thesis

Miller, Andrew Steven



Department of Genetics

The Graduate University of Advanced Studies (SOKENDAI)

December 2017

Abstract

The vertebrate telencephalon, a center for higher-order processing, is vital to the integration of learning, memory, emotion, and sensory inputs. However, the neurological basis of these functions are still not fully understood, particularly in the case of teleosts. In order to understand how the neural circuits essential for these behaviors form, and how these circuits may ultimately produce sophisticated behaviors, larval zebrafish can be used as a model to visualize the activities of neurons in the process of establishing functional circuits, as well as during stimulus processing and behavioral tasks. Since the transparency of zebrafish larvae allow light to pass through the entirety of their brains, living specimens may be used for optogenetic studies without the need for invasive tissue dissection. Furthermore, in the initial stages of brain development, the telencephalon exhibits activities generated by internal processes, rather than by external stimuli. These spontaneous activities are believed to be indicative of the types of activity observed in later, mature neural circuits, and therefore formed the basis of my analysis. Using Genetically Encoded Calcium Indicators (GECIs) such as GCaMP expressed in genetically defined portions of the forebrains of 5 day old zebrafish through the Gal4/UAS system, I recorded activities of neural populations of agarose-fixed larvae under a confocal microscope. I then proceeded to use dimensionality reduction and signal analysis techniques to find consistent patterns among them, identifying a population of cells with slow, periodic oscillations alternating at a rate of approximately 0.1 Hz between the left and right hemispheres of the dorsal surface of the forebrain. Using a custom analysis pipeline to register confocal imaging data from multiple optical layers and fish, I was able to expand this analysis to the more ventral optical sections of the dorsal telencephalon, finding a gradient of frequencies across the anteroposterior axis of the pallium consisting of cells with progressively slower periodic activities towards the posterior end. In order to elucidate the mechanics of these oscillating cells, and their possible behavioral

functionality, I attempted to manipulate the frequency and phase of the oscillator through pharmacological and visual stimulus-based interventions. Treatments of baclofen, a GABABR agonist, resulted in a reduction in the 0.1 Hz activities of the oscillating telencephalic cells, fitting with an oscillating circuit model that would require inhibitory inputs to both hemispheres to maintain a separation in terms of phase. Moreover, with a visual stimulus protocol consisting of periodic dark flashes displayed in an alternating fashion to the left and right eyes of the larvae, I was able to identify populations of neurons in both the telencephalon and optic tectum with initially periodic, spontaneous alternating activities that were also responsive to the phase of visual stimuli. In the case of the visually responsive telencephalic cells, a difference in sensitivity to left or right-sided stimuli was also found, based on the initial phase of their ongoing spontaneous activities. Additionally, the telencephalic pallium contained a smaller population of cells that were responsive to visual stimuli from both the left and right eyes. Since both of these populations were capable of entrainment after the end of visual stimuli, this suggests that these cells may be part of a circuit able to integrate visual information over short time-scales, similar to functionalities proposed for another recently identified oscillator in the larval zebrafish located in the hindbrain, and implicated in long term biases in swim directions. The shared frequencies and similar responses to visual input suggest that these two oscillators may in fact be part of a much larger functional circuit. Finally, in order to further investigate the link between telencephalic oscillatory activity and behavior, I developed a system for performing virtual reality behavioral assays on agarose-fixed larvae, using a camera-based method to track tail movements in order to reconstruct intended paths during fictive swim bouts, with the intent to combine it with a calcium imaging platform for future experiments.

Table of Contents

Abstract	1
Table of Contents	3
Chapter 1: Introduction	7
Chapter 2: Spontaneous Activity in the Developing Zebrafish Forebrain	10
2.1 <i>Introduction</i>	10
The Zebrafish Telencephalon	10
Spontaneous Activity	11
Genetically Expressed Calcium Indicators	12
2.2 <i>Aim</i>	13
2.3 <i>Materials and Methods</i>	13
Construction of Transgenic Lines	13
Calcium Imaging and PCA	14
Periodic Averages and Heat Maps	15
Alternate Dimensionality Reduction Techniques	16
2.4 <i>Results: Patterns of spontaneous activity in the developing forebrain</i>	17
Left and Right Hemispheres of Dorsal Forebrain Exhibit Slow Alternating Oscillations	17
Phases of Alternating Periodic Signals Not Captured by jPCA	20
2.5 <i>Discussion</i>	22
Spontaneous Alternating Oscillations- possible origins and functions	22

Network Structure	23
PCA Interpretation	25
On the Use of Periodic Averaging	26
Chapter 3: Whole Brain Analysis	27
3.1 <i>Background</i>	27
The Role of “Big Data” in Neuroscience	27
Functional Staining and Electron Microscope Circuit Reconstruction	28
Whole Brain Spontaneous Activity Maps	30
3.2 <i>Aim</i>	30
3.3 <i>Materials and Methods</i>	31
Recording setup	31
3.4 <i>Results</i>	32
Anteroposterior Gradient of Frequencies in Telencephalon	32
Consistency of Spontaneous Activity over Habituation Period	35
Frequencies of Spontaneous Activities are Relatively Consistent on a Per Cell Basis, and Log-Normally Distributed	37
3.5 <i>Discussion</i>	39
On Inter-peak Interval Distributions	41
On Registration	42
Chapter 4: Manipulation of Oscillations	43
4.1 <i>Background</i>	43
Entrainment and Phase Locking	44
Neural Oscillations and Visual Perception	44

4.2	<i>Aim</i>	45
4.3	<i>Materials and Methods</i>	46
	Pharmacological Manipulation of Spontaneous Activity	46
	Visual Entrainment Protocol	46
	Spontaneous/Evoked/Entrained Activity Assay	47
	Linear Models and Average Activity per Period	48
	Activity Consistency Thresholding	49
	Phase Analysis	50
4.4	<i>Results</i>	50
	Baclofen Treatment Reduces Spontaneous Activity	50
	Visual Stimuli-based Entrainment of Telencephalon Activity	51
	Ongoing Spontaneous Activity and Visual Entrainment	53
4.5	<i>Discussion</i>	58
	On Pharmacological Experiments	58
	On Visual Entrainment	58
	Possible Models	60
Chapter 5: Closed Loop System for Larval 2D Navigation		62
5.1	<i>Background</i>	62
	Behavioral Repertoire of Zebrafish Larvae	62
	Closed Loop Behavioral Assays	63
5.2	<i>Aim</i>	65
5.3	<i>Materials and Methods</i>	65
	Closed Loop Assay Setup and Behavioral Protocol	65
	Optimization of Simulation Parameters	68

Virtual Reality Navigation Assay	70
<i>5.4 Results</i>	70
Larvae Show Expected Avoidance Behavior in Closed Loop 2D Navigation System	70
<i>5.5 Closed Loop System for Larval 2D Navigation</i>	72
Chapter 6: Conclusion	74
<i>6.1 Dynamics of spontaneous activity in the larval zebrafish telencephalon</i>	74
<i>6.2 Effect of visual input on telencephalon oscillations</i>	75
Acknowledgements	78
Bibliography	79

Chapter 1: Introduction

In the field of behavioral neuroscience, a discipline devoted to the question of how behaviors are ultimately produced by the collective actions of neurons, studies may focus on one particular level of detail, ranging from the analysis of single neuron dynamics to higher-order descriptions of behaviors themselves. Straddling these levels is the subfield known as systems neuroscience which encompasses the mesoscale of neural circuits, or groups of connected neurons that achieve a specific function. Some particularly elegant examples of these circuits include motion detection circuits, which were hypothesized and modeled¹ long before they were observed in actual sets of connected neurons², or the contralateral projections of Mauthner cells to motor neurons in the spinal cord in teleosts³, which achieve a reflexive escape behavior in the opposite direction to touch stimuli. During my studies, I became fascinated by examples of neural circuits like these, and the ways in which their computations could result in effective behaviors. This eventually led to an interest in seemingly complicated behaviors such as navigation and memory, and how these functions may be represented in the brain.

Zebrafish larvae, in particular, seemed perfectly suited for investigations into the development of circuits responsible for behaviors. Transparent and small enough for the entire brain to be noninvasively imaged using optical microscopy techniques⁴, larval zebrafish also demonstrate a number of remarkably sophisticated behaviors during their first week of development, including tracking and anticipating the paths of prey, avoiding looming shadows⁵, and integrating information at short time scales to navigate around areas of darkness⁶. During this same time period, as mid and long range axonal connections are being established⁷, areas of the larval zebrafish brain may be highly active, even in the absence of

stimuli. Notably, the telencephalon, or forebrain of the larval zebrafish exhibits rapid, seemingly random patterns of activation, the functionality of which is presently unknown. I therefore began the task of characterizing these activities, and will describe my findings in the following chapters.

The main goal of my study was to examine the nature and possible functional significance of the spontaneous neural activity present in the forebrain of zebrafish larvae. In order to do so, it was necessary to increase the scale of my analytical methods, creating analysis pipelines to compare frequency data from multiple fish at whole-brain scales. For this segment of the project, the main questions that I wanted to answer were to what degree were the patterns of spontaneous oscillations that I found random or unique to each individual larvae, and if these activities were consistent, whether they related to the actions of other known oscillators in the larval zebrafish brain. Finding highly conserved patterns of activity among a number of larvae would imply that tightly genetically defined patterns of connectivity, rather than stochastic connections made on a functional basis, were the source of these activities. Likewise, demonstrating a connection to the activities of other known neural oscillators would give insight into possible functionalities for the activities of the telencephalon, as functional outcomes for these circuits have already been proposed. For example, the cerebellum of larval zebrafish at this stage exhibits slow oscillations⁸ at a similar rate to those I found in the telencephalon, although functionally has been speculative, with models suggesting possible uses in regulating spontaneous motor activities to produce optimum foraging patterns⁸, or integrating visual information over time for phototaxis⁹.

However, finding the extent and consistency of these oscillations was only the first step. In order to further address the problem of functionality, I attempted to manipulate the phase of the telencephalon oscillator to further understand its possible mechanics. While

doing so, I aimed to specifically answer whether the oscillations were influenced by external stimuli, and if so, how this may drive useful behaviors.

In order to more fully demonstrate the link between the oscillatory activities of the telencephalon, its recruitment during visual perception, ultimately its relation to behavior, I desired to create a system for virtual reality behavioral assays in larval zebrafish, hoping to integrate it with a calcium imaging platform. In the process of developing this system, it was necessary to determine whether the fictive swim motions of the non-paralyzed larvae could be used to reconstruct their intended swim paths in real time, and whether the fixed larvae were capable of demonstrating expected behaviors in this restricted system.

Finally, I will summarize my findings, and attempt to place them into a broader context. While my results do not yet explain the full extent of the neural circuit or circuits involved in the generation of the spontaneous oscillations present in the telencephalon, I hope that this work will form the basis for further studies exploring their mechanics and functionality.

Chapter 2: Spontaneous Activity in the Developing Zebrafish Forebrain

2.1 Introduction

The Zebrafish Telencephalon

In vertebrate brain development, the most rostral portion of the neural tube, or prosencephalon, eventually forms the diencephalon and telencephalon¹⁰. The telencephalon, distinguishable by its distinctive bilobed structure, is separated into bilaterally symmetric left and right hemispheres (Figure 1.A). The telencephalon is also notable for the diverse set of functions performed by its different regions, including olfactory processing, memory and learning, navigation, and emotional processing in teleosts¹¹. In mammals, the telencephalon undergoes an invagination process during development, forming the cerebrum. In contrast, the telencephalon of teleost fish everts during its process of development, complicating the process of locating regions homologous to those in the mammalian brain through anatomical means¹².

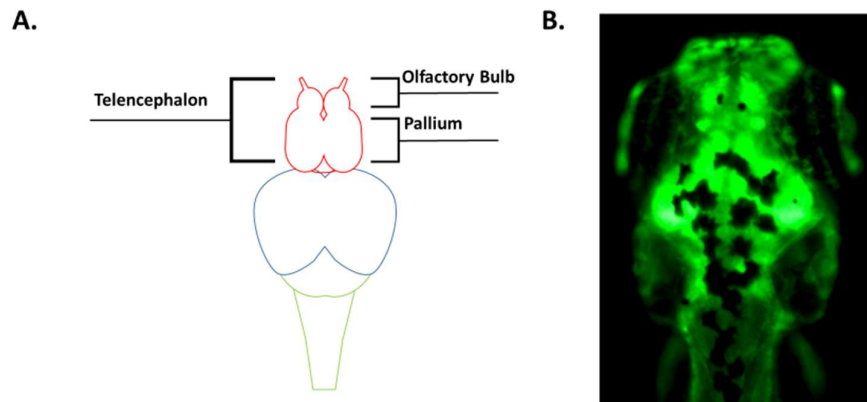


Figure 1. The Larval Zebrafish Brain. **A:** Schematic of the zebrafish brain, dorsal view. The telencephalon, optic tectum, and midbrain/hindbrain are outlined in red, blue, and green respectively. **B:** Dorsal view of the head of a gSAGFF49A zebrafish larva at 5 dpf, expressing GFP in the optic tectum and telencephalon. Pigment cells are visible in the image as darkened portions which are dorsal to the tectum and hindbrain.

Spontaneous Activity

Spontaneous activity, defined as neural activity occurring due to interactions mainly between local neuron populations, rather than external stimuli, occurs early in the process of brain development, as synaptic connections between neurons begin to form, and the density of arborizations increases. Activities between interneurons often take on patterned forms, including moving waves of activity in retinal neurons, or oscillating patterns of activity that may be initiated by pacemaker neurons, or even by particular network arrangements¹³.

While interactions between genetic and activity-based growth factors during development may be complex, correlations between neurons exhibiting spontaneous activity may be used to infer their functional connectivity at early developmental periods¹⁴⁻¹⁶.

Genetically Expressed Calcium Indicators

Although electrophysiology has traditionally been the preferred method of measuring neural activities due to its high temporal resolution, which is capable of distinguishing individual neural firing events, the technique remains limited in terms of the total number of neurons that can be recorded simultaneously. For the identification of functional circuits in animals with massively complicated arrangements of neurons, this is a highly limiting factor, and although progress has been made towards the creation of arrays with multiple probes for electrophysiology¹⁷, optogenetic techniques have become the tool of choice for multi-neuron recording¹⁸.

GCaMP, a genetically encoded calcium indicator (GECI) is composed of the subunits GFP, M13, and calmodulin, which undergoes a conformational change in the presence of calcium ions (Ca^{2+}), increasing the level of fluorescence of the GFP¹⁸. Expressing this indicator in the membranes of neurons allows for the imaging of firing activity, as intracellular calcium levels rise with increasing rates of action potentials. This is reflected as a linear increase in fluorescence in GCaMP, producing a signal which can then be deconvolved to approximately reconstruct the original pattern of neural spikes¹⁹. By expressing GECIs through techniques such as the creation of enhancer traps via Gal4/UAS to target particular brain regions, or by pan-neuronal promoters to visualize activity in all parts of the brain at once²⁰, it becomes possible to analyze neural activity dynamics that take place

on larger scales, involving interactions between cells in circuits as they perform functional computations.

2.2 Aim

I initially became interested in the telencephalon of larval zebrafish due to observing the high frequency, seemingly chaotic neural activities that begin manifesting in the region during early stages of development. Wanting to understand the origin and possible meaning of these activities, I decided to pursue a series of related projects combining optogenetic imaging methods and neuroinformatic analysis techniques.

2.3 Materials and Methods

Construction of Transgenic Lines

Candidate Gal4 lines with known telencephalic expression patterns during the larval stage were screened for strong and consistent pan-telencephalon labeling over a 10 day period of development after being crossed with UAS:GFP. Of these 11 lines, gSAIzGFFM119B was selected due to its strong and consistent pan-neuronal expression of GFP in the telencephalon over the duration of this screening period, and were used in conjunction with the gSA2AzGFF49A and HuC promoter lines. gSAIzGFFM119B, which exhibited a pan-neuronal expression pattern in the pallium until at least day 5 of development (Figure 2.B), remained a line of particular interest due to its inclusion of additional neural subpopulations in the optic tectum and cerebellum. For the purpose of characterizing and comparing the expression pattern of this line, three gSAIzGFFM119B;UAS:GFP larvae were

imaged at 5 DPF under 40x magnification using a confocal microscope (CSU-W1, Yokogawa Electric Corporation). For further chapters, the specific numbers of fish used in each experiment and their genetic backgrounds are described in each respective methods section.

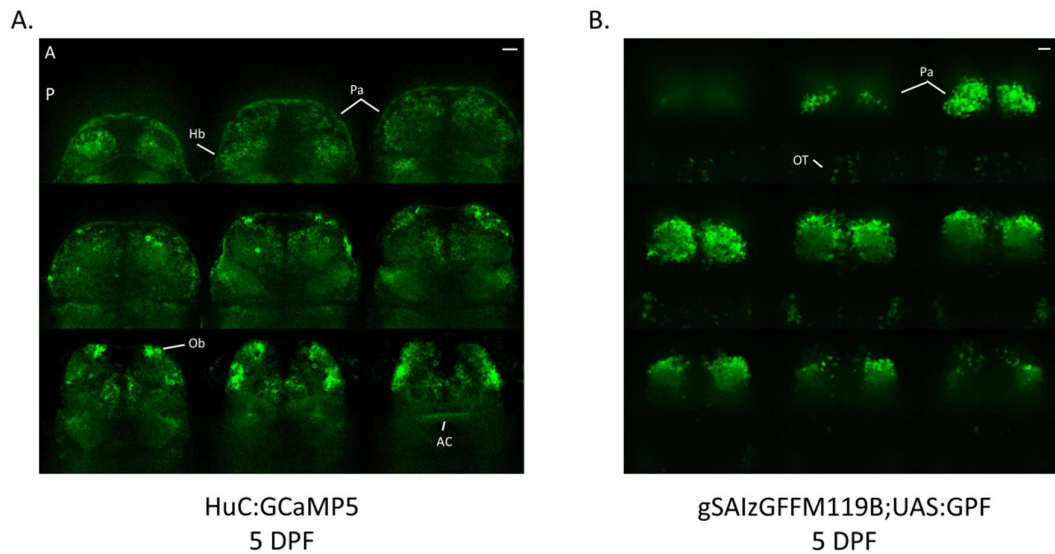


Figure 2. Comparison of Transgenic Line Expression Patterns. A, B: Optical planes from two representative larvae covering the extent of the telencephalic pallium, proceeding ventrally from the pallium's dorsal surface. Scale bars represent 20 μ m. Anatomical landmarks are labeled for reference. Hb: Habenula. Pa: Pallium. Ob: Olfactory Bulb. AC: Anterior Commissure. OT: Optic Tectum.

Calcium Imaging and PCA

Forebrain activity was recorded from 5 day post-fertilization (DPF) zebrafish larvae on a nacre (pigment-less) background expressing GCaMP 5G, either pan-neuronally via a

HuC promoter, or via Gal4 lines with specific expression in the telencephalon. 5DPF larvae were placed in 2% low-melting agarose, immobilizing the larvae, which was then covered with E3 buffer solution once the agarose had set. A confocal microscope with a 40x water immersion objective lens and 488 nm excitation light were used for imaging. Prior to calcium activity imaging, z-axis stacks of the entire forebrain of each fish were made for later anatomical reference. Video recordings were then taken, recording spontaneous activity at different optical sections in the pallium of the telencephalon for 5 minutes at a rate of 10 frames per second. In total, 40 video recordings were taken from 8 HuC:GCaMP5 larvae at 5DPF. Data from 3 recordings of one gSA2AzGFF49A larva and two HuC larvae are shown as examples in the figures of this chapter.

Analyses of the calcium transients were performed by generating separate regions of interest (ROIs) for each cell using CellSort²¹, toolbox employing PCA and ICA to identify individual cells from calcium imaging videos. The spatio-temporal bias of the ICA was set at the recommended default of 50%, and a minimum area of 20 square pixels was used as a criteria for the segmentation of sufficiently large ROIs. Additionally, I created a custom MATLAB script to combine ROIs that had been duplicated due to insufficiently elastic image registration, with adjacent cells having centroids that were closer to each other than the diameter of a single cell merged into a single ROI. For the principal component analyses of the calcium transients from each imaged cell population, the number of components in each data set was determined via scree test.

Periodic Averages and Heat Maps

Periodic averages were calculated by normalizing each cell signal into a z-score (defined as subtracting the mean of each signal and dividing by its standard deviation), and

splitting the z-scores into segments the length of a particular period of interest. The segments were then averaged to produce a mean value for each cell at each time point of the period, displayed in the form of a row-wise heat map.

The rows of each heat map, which represented periodic averages from specific cells, were sorted by either cell centroid positions on an anatomical axis or by their patterns of activity. Activity-based sorting methods included hierarchical clustering, and sorting center of gravity or by peak intensity, as described in each figure. Hierarchical clustering was based on the creation of a dendrogram with Pearson correlation as a distance measurement, and leaf sorting to minimize distances between successive cell averages. To capture the possible effect of sustained up or down states that would otherwise be missed through sorting by a single point of maximum intensity, centers of gravity along the time axis were calculated by first positively rectifying the z-scores of each cell average, then sorting cells by their intensity-weighted central point of gravity along the time axis. This calculation was performed similarly to the case of a series of weights on a one-dimensional balance beam: the masses (signal intensities) of individual weights were multiplied by their distances from the origin, and then their sum was divided by the total mass, resulting in a mid-point of balance.

Alternate Dimensionality Reduction Techniques

For the purpose of jPCA analysis²², an example data set of calcium transients from 22 neurons in the left and right hemispheres of the dorsal telencephalon was used, having displayed slow alternating oscillations in the periodic averaging analysis. The ‘Soft’ normalization function of the jPCA toolbox²² was used, with medial z-scores of 4 mapped to a value of 0.5 and progressively higher scores were kept below a value of 1. For the smoothed data, signals were filtered using a Gaussian function ($\sigma=10$).

Mock data for use in the in the jPCA analysis was made by generating 22 signals composed of a series of periodic impulses occurring at approximately 0.1 Hz (every 100 frames for a frame rate of 10 frames per second), with placements jittered using normalized noise ($\sigma=5$). The impulses were convolved with a Gaussian function ($\sigma=10$) and half of the signals were shifted in phase by 180 degrees, creating two populations of semi-periodic oscillators with alternating activities.

2.4 Results: Patterns of spontaneous activity in the developing forebrain

Left and Right Hemispheres of Dorsal Forebrain Exhibit Slow Alternating Oscillations

In dorsal and medial optical sections of fixed 5dpf 49A and HuC larvae, I observed moderate ($>0.3 R^2$) values between calcium signals from neurons between the left and right hemispheres of the brain. Principal component analysis of calcium signals from the dorsal surface of the telencephalon from a 49A larva revealed four components explaining a large portion (72%) of the total variance of the analyzed cell population. The first component (explaining 39% of the total variance) corresponded to the highly correlated activity of anterior neurons shown in figure 3.C, and the second component to oscillatory activity between the two hemispheres. In principal component 2 (which accounted for 14% of the total variance), cells with positive and negative loadings tended to cluster in each hemisphere (Figure 3.C). Components 3 and 4 meanwhile, appeared to preferentially label ROIs containing neuropil, rather than cell bodies. Measuring the autocorrelation of the second component indicated a high degree of periodicity, with a characteristic sine wave pattern appearing on the graph of autocorrelations at different periods of lag (Figure 3.B), indicating

that the signal had higher amounts of correlation with itself at fixed, regular intervals. The peaks of this autocorrelation occurred at regular intervals of 110 frames, suggesting that the neurons in this component have an 11 second oscillatory cycle occurring in a hemisphere alternating pattern.

Cells with peak levels of activity during different points of the oscillatory cycle could be visualized by the use of periodic averages (Figure 3.D), which revealed two main clusters corresponding to cells in the left and right hemispheres of the dorsal telencephalon when sorted by similarity. However, while cells in more ventral portions of the telencephalon exhibited clusters that were distributed across the oscillatory cycle (Figure 3.E), these clusters contained cells from both the left and right hemispheres.

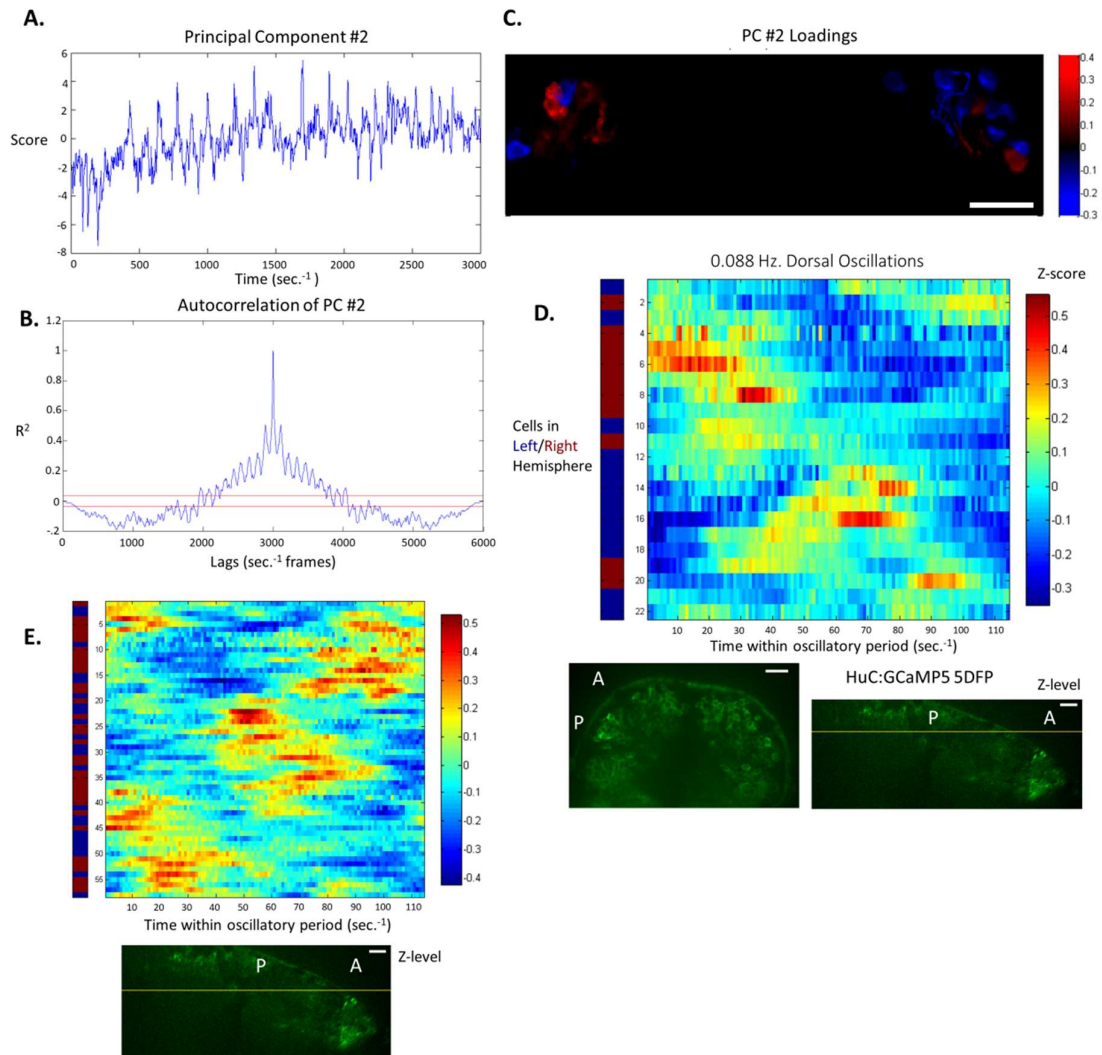


Figure 3. Calcium Signal Analysis. **A:** Scores for principal component 2 of a set of neurons in the dorsal telencephalon of a 49A larva, over 5 minutes of calcium activity. Scale bars represent 20 μm . **B:** Autocorrelation of the principal component 2 signal from A, over 6000 lags. The 95% confidence intervals are shown in red. **C:** Loadings of each cell on principal component 2, with positive loadings shown in red, and negative loadings shown in blue. **D:** (Above) Period-aligned average activities of cells in a dorsal telencephalon section from a HuC larva, displayed as rows in heat map colored by z-score. Left/right hemisphere placement of cells is shown on the accompanying left bar. (Below, left) Image of layer used

in analysis above (Below, right) Transverse section, with imaged layer shown as a yellow line.

E: Period-aligned average activities of cells in central telencephalic pallium.

Phases of Alternating Periodic Signals Not Captured by jPCA

In an attempt to more accurately represent the periodic activities of cell populations through dimensionality reduction, I performed jPCA²² on an example calcium recording of dorsal telencephalon cells found to have alternating periodic activities previously with PCA and periodic averaging. However, the first two principal components of the jPCA projection failed to capture either the expected frequency or phase of the oscillations, regardless of the preprocessing measures used on the original data (Figure 4.A-B), or with shorter timescales.

To test the capability of jPCA to represent alternating periodic activities, I created a simulated data set consisting of two alternating populations of cells with minimal amounts of noise as a positive control (Figure 4.C). While the jPCA projection managed to reflect the 0.1 Hz frequency underlying the original oscillations in the data when the analysis was performed at a shorter time scale of 20 seconds (Figure 4.D), the phases of the two populations were not represented accurately relative to the original phases, or to their relative difference in phase angle (Figure 4.E). Traditional PCA, on the other hand, more accurately captured both the frequencies and phases of the two populations in the first two principal components (Figure 4.F).

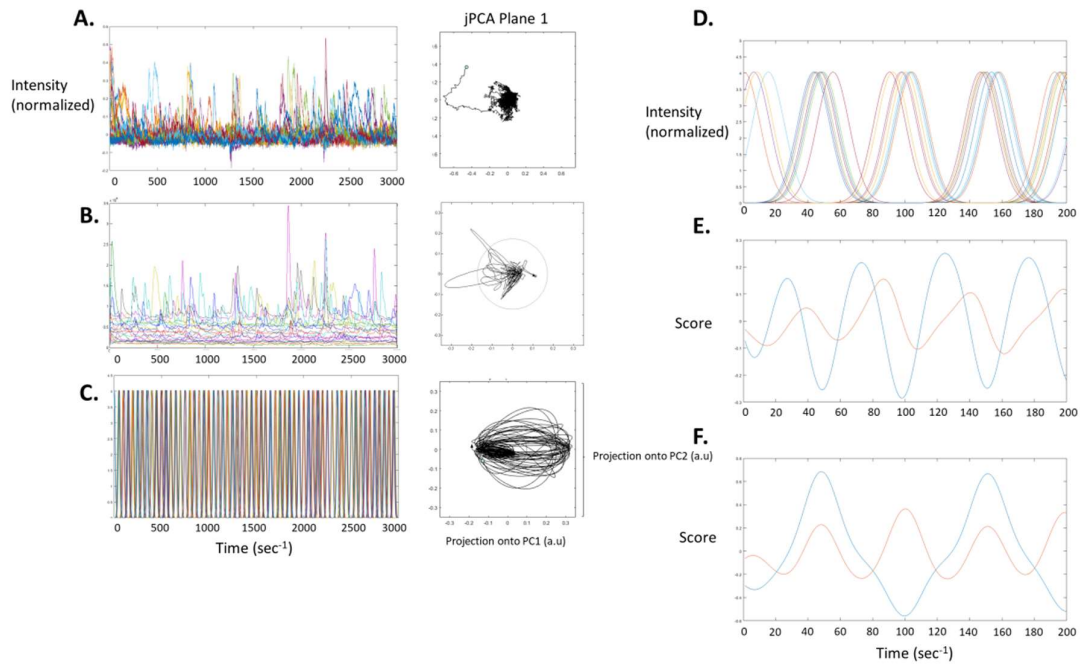


Figure 4. jPCA Projections of Normalized and Mock Data. **A:** (Left) Softmax normalized calcium signals from 22 neurons from an example 5 minute recording of spontaneous dorsal telencephalon activity. (Right) Projection of data into first 2 principal components in jPCA space. **B:** (Left) Same cell signals as in A, convolved with Gaussian kernel. (Right) jPCA Projection. **C:** (Left) Simulated signals from two populations of cells ($N=11$ for each population) with noise jittered alternating patterns of activity at 0.1 Hz. (Right) jPCA Projection. **D:** 20 second long segment of signals from C. **E:** First 2 principal components of jPCA projection for simulated data in D. **F:** First 2 principal components of traditional PCA projection for simulated data in D.

2.5 Discussion

Spontaneous Alternating Oscillations- possible origins and functions

During the process of embryonic and early postnatal brain development in vertebrates, expression levels of the K-Cl co-transporter, KCC2, are lower in comparison to those of mature neurons, resulting in a higher intracellular Cl⁻ concentration. This chloride ion surplus results in a Cl⁻ gradient across the neuronal membrane, and an efflux of Cl⁻ during GABA_A or glycine receptor activation, essentially providing GABA/Gly with excitatory, rather than inhibitory effects during this stage²³. The result of these excitatory GABA/glycinergic interactions are networks with higher basal rates of spontaneous activity, and in areas with recurrent inhibitory projections, characteristic periodic waves of activity known as Giant Depolarizing Potentials (GDPs)²⁴. In preparations of acute slices of postnatal rat hippocampus, GDPs have been observed in bilaterally synchronized waves of activity with a frequency of approximately 0.03 Hz²⁵, as well as in *in vivo* hippocampal recordings of behaving and anesthetized rat pups at rates between 0.033-0.1 Hz²⁶, a similar range to the frequencies observed in the spontaneous activities of the larval zebrafish telencephalon. The oscillations of the zebrafish forebrain may therefore be produced by the same mechanism, with reciprocal GABAergic or glycinergic projections between the left and right hemispheres of the telencephalon producing the alternating bouts of activity.

Aside from a mechanical explanation for the oscillatory activity patterns of the zebrafish forebrain, previously observed oscillators in other parts of the zebrafish brain may indicate a possible functional role for this type of activity. Posterior to the cerebellum are clusters of neurons exhibiting a similar pattern of alternating oscillations at approximately 0.4 Hz.²⁷ These hindbrain oscillations have been shown to correlate with the average swim bout direction of larvae, and may contribute to efficient foraging behaviors during locomotion,

ensuring a wide area of coverage during exploration⁸. While additional studies have shown that left/right hemispheric biases in activity can be induced by unilateral or laterally moving visual stimuli⁹, it remains to be shown whether the oscillations of these hindbrain clusters are generated intrinsically, or modulated by other areas of the brain, leaving the forebrain oscillator as a possible upstream modulator of the hindbrain oscillator through rhythm entrainment, or phase-locking.

Additionally, studies in mice and humans have indicated the importance of hippocampal theta rhythm phase in the association of successive visual scenes or cues occurring in short time frames^{28,29}, raising the interesting possibility of telencephalon oscillations being part of a rudimentary system involved in short term associative memory. As long-term potentiation (LTP) requires associations to be made within a time scale of approximately 20 ms³⁰, repetitions of neural engrams within the troughs of the hippocampal theta rhythm could allow temporally disparate cues to be brought within a feasible range for LTP to occur^{28,29}. Furthermore, such a scheme would have the feature of compensating for more rapid presentations of successive cues due to changes in the animal's movement speed during exploration^{28,29}, as higher frequencies of hippocampal theta waves are associated with the initiation of movement³¹.

Network Structure

A pattern of long-range connections with particular nodes acting as highly connected hubs, as I observed in the correlations between spontaneously active neurons in the dorsal telencephalon, is referred to in network literature as a “small world network,” which in theoretical models has the property of connecting relatively high numbers of nodes with short paths, measured in jumps between nodes³². The disparity between the amounts of inferred

connectivity between forebrain neurons may reflect such an arrangement, with the effect of maximizing connectivity between disparate areas of the developing forebrain.

Clues towards a possible neural circuit structure accounting for the alternating patterns of activity that I observed in the zebrafish telencephalon may lie in previous studies of neural oscillators found in the larval zebrafish nervous system: primary motor neurons in the spinal cord at day 1 postfertilization³³⁻³⁵, and the anterior rhombocephalic turning region (ARTR)⁸. These oscillators, both of which are associated with directional motor movements at different temporal scales, appear to incorporate reciprocal interneuron projections between the alternating clusters, a feature found in many central pattern generators (CPGs) across a number of species³⁶.

In the case of larval zebrafish spinal motor neurons, rhythmic activations are retained after the abolishment of inhibitory transmission, although glycinergic transmission is necessary to produce lateral alternations in activity, suggesting the presence of reciprocal inhibitory glycinergic projections synchronizing each side to opposing phases³⁷. Similarly, immunohistochemical characterization of neurons present in the ARTR, a region associated with alternating biases in overall turn directions during swimming behavior, reveals the presence of separate GABAergic and glutamatergic populations present in both hemispheres, with mutual contralateral projections, the GABAergic interneurons likely fulfilling a similar function by suppressing contralateral activity⁸.

While my current work does not touch upon the cell types responsible for the alternating oscillations of the larval zebrafish pallium, it is likely that a similar motif of mutually inhibitory projections should exist within close proximity to the pallium, with a likely candidate being the anterior commissure (AC) of the subpallium. At days 1-3 postfertilization, a portion of neuron fibers originating from the lateral pallium³⁸ and crossing

the AC have been shown to be immunoreactive to anti-GABA^{38,39}, and positive anti-Gad67 staining in the AC at 6 days postfertilization suggests the continued presence of GABAergic projections between the right and left hemispheres in the subpallium through the larval stage⁴⁰. These inhibitory projections may be outweighed by glutamatergic signals at later stages of development however, as stimulation of the lateral telencephalon in adult zebrafish brain slices induces a negative field potential in the contralateral dorsal medial region, a process that is mediated by glutamatergic transmission through the AC⁴¹.

PCA Interpretation

For the purpose of analyzing high-dimensional data sets, a number of dimensionality reduction techniques exist, each with their own particular use cases. Of these, PCA is notable for its reliance on linearly correlated variables to find dimensions of maximal variance, and the strict orthogonality of its resulting components. For these reasons, it is generally not favored when analyzing data with important non-linear relationships between variables, as some researchers argue is the case in recordings of neural populations⁴². However, given the properties of the oscillator in question, with two populations having equal magnitudes and stable but differing phases, we should expect the relationship between the populations to remain linear. Nonlinear methods would therefore be unneeded to identify simple neural oscillators, and only introduce further complexity into the analysis pipeline. Variants of PCA designed with oscillatory activities in mind may also have their own tradeoffs in terms of applicability. jPCA²², for example, appears best suited to data sets with short periods, low levels of noise, or enough aligned samples to offset its noise sensitivity.

The hemisphere-specific oscillations found on the dorsal surface of the telencephalon were only the second component in the analysis, meaning that the overall fluctuations were

smaller in intensity compared to the activities of a smaller population of highly active anterior neurons, which were positively correlated between the two hemispheres. This fits with the interpretation of the oscillations as the result of up and down states of excitability that are alternating between the left and right hemispheres, upon which other high-intensity activity patterns are overlaid. However, it may also suggest that the primary source of the oscillating up and down states may be from signals received from a separate, directly oscillating circuit with projections to the imaged neurons.

On the Use of Periodic Averaging

While period-based averaging is seldom used for data analysis in neuroscience, with most averages being based around stimulus-onsets or spike-onsets, my rationale for employing this method comes from its similar application in the calculation of light curves in the context of astrophysics⁴³. One commonly used method for detecting exoplanets requires finding regular periods of fluctuation in light intensity for a particular star, which may be obscured by noise from a variety of sources, a problem resembling that of finding periods in a noisy population of active neurons. Periodic averaging may be used in cases where underlying periods in the data may be obscured by noise, and the appropriateness of a particular period length as a basis for the average may be evaluated by similar means: either by use of phase dispersion minimization in time bins for the case of light curves, or by the minimization of variance in each time point of an average, as I have used in my analysis. Essentially, for periodic signals, per-time point variance decreases and the curve becomes more defined as an appropriate period is approached.

Chapter 3: Whole Brain Analysis

3.1 Background

The Role of “Big Data” in Neuroscience

In recent years, considerable efforts have been devoted to large scale projects gathering and integrating functional and neuroanatomical data sets for the purpose of fully mapping neural circuits involved in perception and behavior⁴⁴. The end goal of these “big data” projects, completing a full index of neuron-to-neuron or circuit-to-circuit connections, or “connectome” in a model organism at a particular level of detail, represents one strategy for building an understanding of brain function. Starting from a broad base of data, common motifs would ideally be observed, and hypotheses generated and tested regarding the recruitment of neurons and circuits during behavior through correlational analysis.

Furthermore, whole brain imaging and analysis may in fact be necessary for capturing the activities of long range projections or clusters that cannot be visualized in a single optical plane, or single brain areas⁴⁵. Similarly, whole brain imaging techniques allow for the collection and comparison of large numbers of samples; a necessity if neural structures or functions have stochastic elements. For example, population codes may be assigned on an ad hoc basis and shift over time, rather than being purely based on a genetically defined subpopulation^{46,47}.

Caution, however, must be taken when drawing conclusions based entirely on correlational analysis. Putative circuits may be identified if relevant brain states are captured in the original data set, but specific insights into circuit function⁴⁸ may require new

experiments to tease out causes from effects. Ultimately, researchers wishing to properly understand the functional dynamics of neural circuits may need to combine focused analysis which may then be integrated into a larger context with big data sets.

Functional Staining and Electron Microscope Circuit Reconstruction

Projects focusing on larval zebrafish as a model have included light-sheet based whole-brain imaging of responses to visual flash stimuli⁴⁹, whole-brain immunostaining maps of activity based on immediate early gene (IEG) or phosphorylated extracellular-regulated kinase (p-ERK) expression⁴⁰, and even serial electron microscope sectioning data for connectivity mapping⁵⁰.

Immunostaining, which necessarily requires the use of dissected and fixed tissues, may appear at first glance to be unsuitable for visualizing the activities of functioning neural circuits. However, high levels of neural activity associated with the induction of synaptic plasticity are correlated with rapid increases in expression levels for a number of IEGs, and in-situ hybridization for these gene products may therefore be used as a proxy for activity levels within a particular temporal window^{51,9}. For C-fos and Arc, two common IEGs used for neural imaging purposes, staining against their gene products allows for the visualization of total activity levels over a 1-2 hour long period, and RNA staining is able to narrow this window down further to a period of 30 minutes⁵¹. More recently, phosphorylated-ERK stains, involving the mitogen-activated protein kinase / extracellular signal-regulated (MAP/ERK) pathway associated with synaptic plasticity have been employed in both the juvenile mouse⁵² and larval zebrafish⁵³, producing detectable signals from active neurons within 5 minutes of stimulus presentation or direct CHR2 activation⁴⁰. Because the readout of the activity levels is

essentially stopped in place, the end result is an entire brain “snapshot” of this window that can be analyzed postmortem and integrated into a whole-brain database project- an effort already performed successfully for larval zebrafish exposed to light flash, optomotor, aversive, and prey-capture inducing stimuli⁴⁰. While in some cases, sparse labeling or specific genetic lines may be able to identify conserved neural motifs and circuits, the strength of functional staining lies in its ability to identify active regions on a global scale, rather than in singling out specific projections.

To capture connectivity data on a much finer scale, projects involving electron microscopy of serial sections of brain tissue have been undertaken, with the end goal of producing a synapse level connectome⁵⁴. While the end result provides a highly detailed record of connectivity based on direct anatomical observations of synaptic connectivity, the sectioning and imaging process itself may be slow and costly⁵⁴, even when fully automated⁵⁰. Furthermore, most project workflows rely on manual or semi-automated reconstruction methods to trace projections through the image stack and assign identities for the synapses observed, a time-consuming process that often requires large numbers of volunteers, or unreasonably long durations of time⁵⁴. For this reason, reconstructions of particularly dense arrangements of neurons, such as the visual cortex of the mouse been limited to small volumes so far, reaching sizes of 1,500 μm^3 at maximum⁵⁵. Recent results in the field of machine vision, however, have promised higher reconstruction rates at several orders of magnitude, with error rates gradually approaching those of manual labeling methods^{56,57}.

While the large amount of data produced by serial electron microscopy could be considered a point in favor of the technique, it may also pose its own set of challenges. Aside from the logistical issues of data storage, transmission speeds, and processing power that must be taken into account when working with large data sets⁵⁸, identifying behaviorally

relevant circuits within the entire wealth of connectome data proves its own problem. Electron microscopy data may function as a useful confirmation of putative circuits identified in behavioral experiments⁵⁹, but large scale analyses of connectomes on their own have been limited to characterizations based on network/graph theory⁶⁰ or topology⁶¹. Critics of the practice^{48,54} argue that large-scale collections of data are not a direct path towards an understanding of neural function as it relates to behavior, favoring smaller-scale modeling of neural circuits as computational units- an approach that requires carefully designed experiments and a focus on specific brain regions.

Whole Brain Spontaneous Activity Maps

Although whole-brain imaging techniques have previously been employed to image spontaneous activity in the larval zebrafish brain, these data sets have been recorded at low frame rates with clustering methods unable to capture the periodic activities of the forebrain²⁷, or with horizontal light sheet angles that necessitated the avoidance of the forebrain region due to the presence of eyes on each side parallel to the imaging plane which blocked light transmission^{9,49}.

3.2 Aim

In order to understand the spontaneous activities on the entire larval zebrafish telencephalon, and its possible relationship with the activities of other brain areas, I developed an imaging and analysis pipeline to more easily compare imaging data from multiple brain regions and fish. This pipeline formed the basis both for imaging studies of

spontaneous activities, and later experiments involving perturbations of activities in the telencephalon.

3.3 Materials and Methods

Recording setup

Fifteen 5DPF larvae expressing HuC:GCaMP6s in a nacre background were fixed in 2% low melting agarose and covered with E3 buffer solution in 60 mm. plates for confocal imaging. Of these larvae, six were imaged with a 40x water immersion lens centered on the telencephalon, and the remainder with a 20x water immersion lens providing a whole-brain field of view. Videos of the spontaneous activity of cells at different layers of the pallium of the telencephalon were then taken at 10 frames per second, lasting 5 to 10 minutes each. Individual videos were registered to levels of their respective z-stacks though finding the maximum correlation coefficient between the first video frame, and each z-stack image. Z-stacks of three individual fish were then registered to a reference brain by 3D rigid transformation using the Matlab Image Processing Toolbox.

The fundamental frequencies for each cell were estimated by taking the maximum squared difference between the original calcium signal, and the signal convolved by a series of 2000 notch filters ranging between 0 and 5 Hz⁶². Phase angles were calculated by sorting calcium signals into bins according to their fundamental frequencies at 0.02 Hz intervals, and correlating them against a series of phase-shifted comb filters at matching maximum bin frequencies.

The distributions for inter-peak intervals were determined by first normalizing each cell signal to zero mean. Next, cell signals were divided by the top 0.01 percentile of intensity values for each recording. This step allowed for consistency to be maintained between

separate recording sessions, but also the retention of the relative intensities of each cell. At the same time, the biasing effect of cells with large intensity spikes that were often the result of rare motion artifacts could be avoided. Calcium transient peaks were then identified using the Matlab 'findPeaks' function, with the criteria being a minimum peak width of 7 and a minimum peak prominence of 1.5.

3.4 Results

Anteroposterior Gradient of Frequencies in Telencephalon

Due to the apparent lack of hemisphere-dependent alternating oscillations in mid-to-ventral sections of the pallium occurring at a single frequency, I hypothesized that the spontaneous activities of these cells may exhibit a wider range of intrinsic frequencies. Plotting the estimated fundamental frequency of each cell against its position along the anteroposterior axis (the Y position in the imaging video) reveals a moderate positive correlation ($R^2= 0.3174$) (Figure 5.A-C). This anteroposterior gradient was consistent across different depths of the pallium, as well as between the multiple fish used in the imaging experiments (Figure 6.A-D).

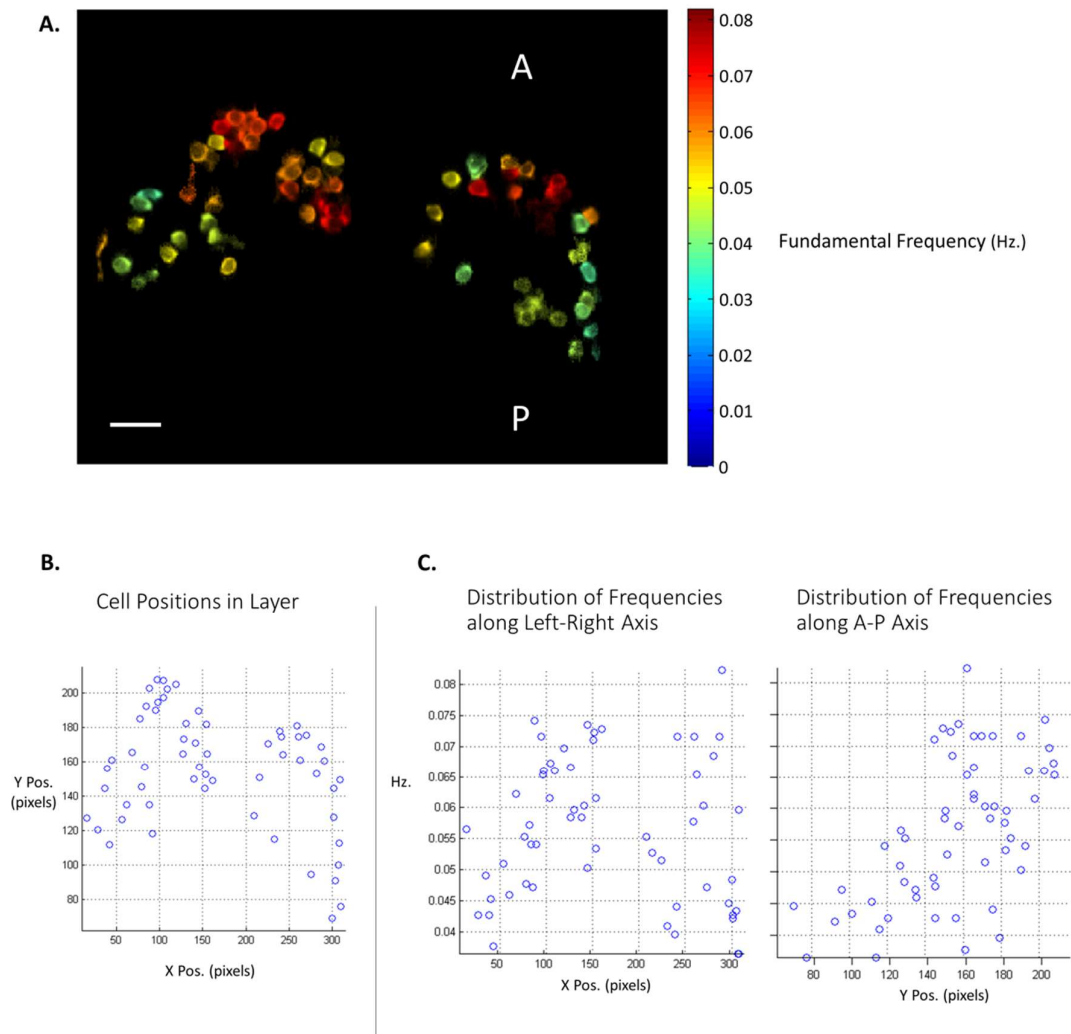


Figure 5. Distribution of intrinsic frequencies. **A:** Fundamental frequencies of cells in ventral layer of pallium, colored by fundamental frequency. The scale bar represents 20 μm . **B:** Centroids of cells shown in A, with more anterior cells shown at higher Y values. **C:** Scatterplots of fundamental frequencies of each cell, charted against their X and Y (A/P axis) positions.

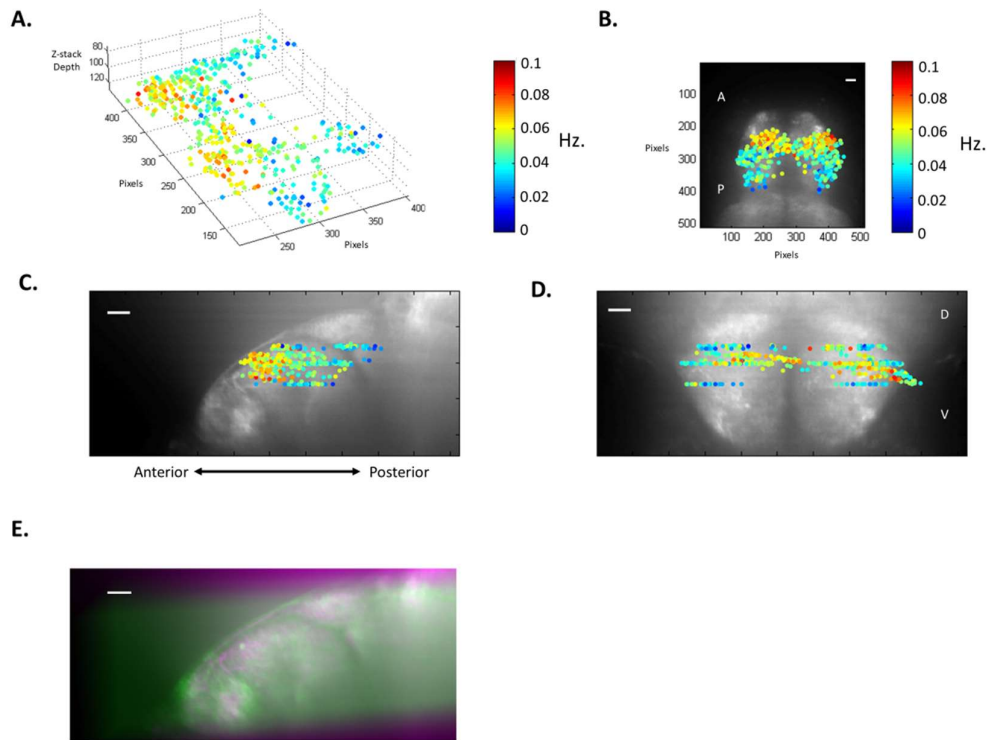


Figure 6. 3D Registration of Frequency Data for Multiple Fish Brains. **A:** Whole-telencephalon fundamental frequency data from 3 aligned larvae. Spots indicate cell centroids, and are colored by fundamental frequency **B,C,D:** Orthogonal views (horizontal, sagittal, and coronal planes) of point cloud shown in A, displayed against anatomical reference stacks. Scale bars represent 20 μm . **E:** 3D registration of two example anatomical z-stacks (shown in magenta and green) used in the aggregated data set (sagittal view).

Consistency of Spontaneous Activity over Habituation Period

Testing the effect of additional habituation time on the intrinsic frequencies of spontaneously active neurons was crucial during the process of optimization for the imaging protocol, since multiple layers in a single fish are imaged sequentially in a given recording session, and videos of later layers may be taken up to an hour after the start of the experiment. A single z-layer was imaged after the fish was initially positioned under the confocal microscope, and then re-imaged after a 30 minute habituation period in darkness, without the fluorescent excitation light. While the automatically generated ROIs for each video differed (indicating a possible reduction in cell fluorescence below an automatic detection threshold), the intrinsic frequencies of the majority of the cells were not significantly altered, as shown by a comparison of the pre and post-habituation videos using the same ROIs generated by the initial video (Figure 7).

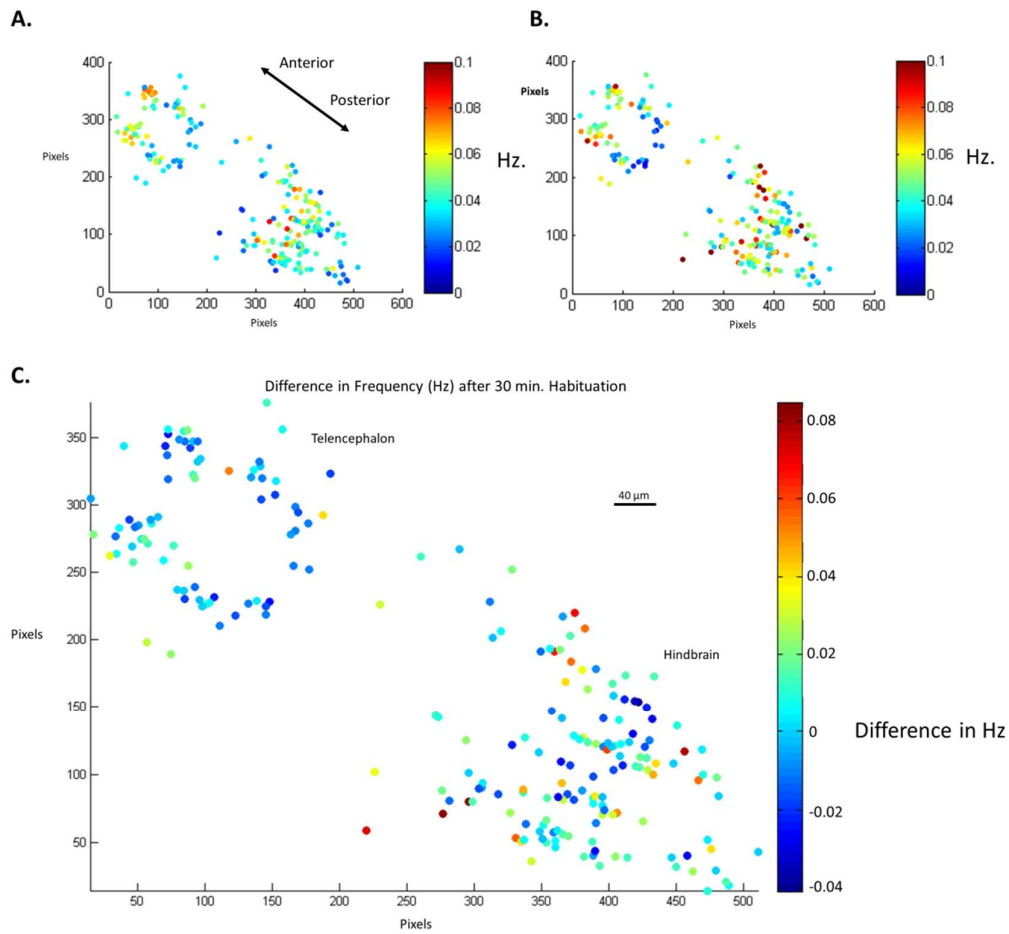


Figure 7: Effect of Habituation on Intrinsic Frequency. **A:** Intrinsic frequencies of neurons from a single horizontal layer of entire brain. Anterior and posterior clusters represent the telencephalon and hindbrain respectively. **B:** Frequencies of cells in ROIs from A, after 30 minute dark habituation. **C:** Difference in frequency between A and B, on a per-cell basis.

Frequencies of Spontaneous Activities are Relatively Consistent on a Per Cell Basis, and Log-Normally Distributed

As the previous method of frequency fitting assigned a single frequency to every cell without a measure of consistency other than the relative size of residuals after filtering, I decided to measure the intervals between activity peaks in order to view their distributions directly. Within single recordings of spontaneous activity (Figure 8.A) and among different optical layers of the telencephalon (Figure 8.B), most cells exhibited intervals that fell within a relatively narrow range, with a mean falling into the range of 100-200 frames (or 10-20 seconds). Longer intervals tended to be uncommon, and the general distribution of intervals was best approximated by a lognormal distribution (Figure 8.C-D).

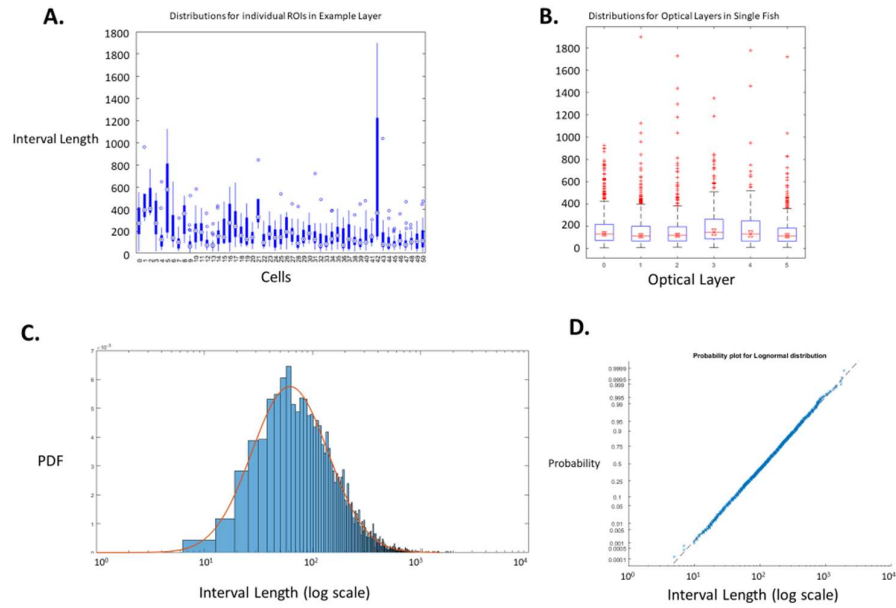


Figure 8: Distribution of Inter-peak Intervals **A:** Distributions of inter-peak interval lengths for 51 cells in one example optical layer of the telencephalon. **B:** Distributions of intervals for 6 optical layers spanning the dorsal to ventral extent of the pallium, recorded from a single fish. **C:** Probability distribution for all intervals (N=3627) from all layers of a single fish, fitted with a lognormal distribution ($\mu=4.78$, $\sigma=0.81$). **D:** Probability plot of data from C against lognormal distribution.

3.5 Discussion

Spontaneous Activity Frequency Gradient

The presence of an anteroposterior frequency gradient in the rates of spontaneous activity in pallial cells calls into question both the developmental origins of this organization, and its possible functionality. Considering the locations of proliferation zones in the developing pallium, one possible explanation for the gradient could be a birth order effect. Fate mapping experiments have shown an elongation of the larval zebrafish pallium along the anteroposterior axis from days 2-5 postfertilization, with proliferating cell populations appearing at the posterior wall of the telencephalon at day 2, and along the dorsal surface of the pallium on subsequent days¹². Cells located towards the anterior pallium are therefore likely to be progressively older than those in the posterior, which may account for differences in their rates of spontaneous activity at day 5. However, my observations of spontaneous activities in day 6 larvae did not appear to show increased rates of activity for medial and posterior pallium cells, suggesting that birth date may not be the only factor contributing to the appearance and maintenance of the frequency gradient. One possibility may be differing passive membrane properties, which in the posterior zone of the pallium of the adult zebrafish have been shown to act as a low-pass filter for the high frequency oscillatory input they receive from mitral cells during olfactory stimulation⁶³. However, the properties of these neurons at the larval stage, or those of more anterior pallial cells have yet to be examined in depth.

For now, we may be uncertain of any behaviorally relevant functionalities for this particular distribution of activity rates, but we may speculate based on examples of brain areas with similarly arranged topographies, as well as the currently known functionalities of other oscillators in the larval zebrafish brain. During early development, the zebrafish optic

tectum displays neural assemblies clustered by spontaneous activity patterns into single-hemisphere sections and bilateral strips laid across the rostral-caudal axis⁶⁴. As the clusters' positions along the rostral-caudal axis of the tectum corresponded to the azimuths of their areas of maximum response for their eventual receptive fields, this provides an example of the topography of spontaneous activity acting as a precursor to functional retinotopy, and a reinforcement of the arrangement by strengthening local connections within clusters⁶⁴.

One additional possibility, albeit much more speculative in nature, is that a range of oscillations occurring at differing frequencies could support the integration of stimuli at multiple time scales through varying rates of sampling. Experiments involving changes to the intensity of whole-field illumination based on the gaze direction of zebrafish larvae have shown that larvae are capable of using information integrated over short time-scales to bias swim bouts towards the direction of diffuse light sources⁹. Since the overall gaze direction is associated with the phase of the ARTR, which in turn can be affected to a certain degree by visual input, this system demonstrates the possibility of alternating oscillations being used in service of a navigational strategy. However, many parts of the circuit responsible for this behavior are unknown. Due to the overlap in time scales for the ARTR and the oscillations of pallium cells, they may provide flexibility to account for time scales ranging between 10-20 seconds, as inter-bout intervals during spontaneous exploratory swimming are also variable, tending to range around 1-5 seconds⁶⁵.

Inter-fish Comparisons

When comparing neural imaging data from multiple individuals, it is necessary to insure that conditions are as similar as possible. Unlike behavioral experiments with defined start times based on displayed stimuli, that would in theory produce consistent results,

recordings of ongoing spontaneous activity are by necessity started at random points of the ongoing cycle, resulting in series of trials with an unknown but theoretically even distribution of phase angles. Some solutions to this problem include recording longer sessions for a clearer analysis of single trials, using phase-free metrics, aligning multiple time series by phase fitting, or redesigning experiments to include defined time points as a basis for analysis. While this current chapter focuses on the first two strategies, with attempts at phase fitting somewhat stymied by low signal to noise ratios, the next chapter approaches this issue by employing presentations of visual stimulus as a fixed reference point.

On Inter-peak Interval Distributions

Unlike the previously discussed methods of periodic averaging and frequency fitting, measures of inter-peak intervals are able to describe semi-periodic cells, or cells that change frequency over time, either by drifting or in response to stimuli, as wider unimodal or multimodal distributions respectively.

One important point to note is the lognormal distribution of intervals found in the larval zebrafish telencephalon. While individual cells displayed relatively consistent firing rates that appeared normally distributed (Figure 8.A), the skewed distribution of cells with fast and slow rates of activity resulted in the long-tailed distributions evident in Figure 8.A and B. Lognormal distributions in firing rate have been previously observed in a wide variety of cortical neurons, ranging from principal neurons in the rat hippocampus to populations of principal neurons and interneurons found in the parietal reach region of the macaque^{66,67}.

On Registration

One possible area of improvement in the comparison of data sets from multiple fish would be the use of an elastic image registration framework⁶⁸. As the sizes and precise shapes of brain areas in larval and juvenile fish can vary due to differences in development (with cell placement in early stages of telencephalon development especially prone to stochastic influences), a more accurate method of registration that compensates for localized differences may allow for the identification of functional neural subpopulations at a finer resolution. However, one-to-one correspondences for individual neurons between individuals may be difficult except for cases in which neuron morphologies are distinctive and their characterization is already well described, as with Mauthner cells in the larval zebrafish hindbrain⁶⁹, or with the use of highly specific gene trap lines⁷⁰.

Chapter 4: Manipulation of Oscillations

4.1 Background

Models of Neural Oscillation and Synchrony

Models of oscillatory phenomena have been widely studied in physics, but at their most basic, regular oscillations can be analogized to the simple motions of undamped pendulums. A system of multiple interacting oscillators, then, may be modeled as a series of pendulums, each initially moving at its own intrinsic frequency, with spring forces between them representing their respective degrees of coupling. This scheme, formalized in the Kuramoto model, predicts that synchronizations in the frequency and phase of the oscillators, or “phase-locking,” will occur for sufficiently high values of mutual interaction⁷¹. With additional rules added to the model, such as a sigmoid weighting function favoring oscillators close to each other in terms of phase, configurations like two clusters appearing in opposite phase can be observed⁷². Although only attractive forces are present in the model, clusters approximately 180 degrees in phase from each other are mutually unaffected, and are therefore allowed to remain separate without coalescing into a single phase.

Models of the dynamics of single neuron membranes may also exhibit regular patterns of firing or burst trains in isolation^{73,74}, furthering the applicability of the Kuramoto model to populations of synchronized neurons, which may have individual preferred frequencies⁷⁵. The intrinsic frequencies and phases for a population of active neurons may shift over time depending on their level of functional connectivity, approaching a state of synchrony enforced by the activities of their neighbors.

Entrainment and Phase Locking

In order to quantify and model oscillatory signals from real-world sources such as neural activities, which are often obfuscated by the presence of noise and additional frequency components, frequency components of interest must be isolated from the total data. To this end, a variety of frequency decomposition and phase fitting methods have been employed in the analysis of electrophysiological signals and imaged calcium transients.

While the Fourier transform is the most well-known of these methods, decomposing signals into a series of component sine and cosine waves, other similar techniques such as wavelet transforms and the Hilbert transform have added to the set of analytical tools used in neuroscience research due to their increased performance with irregular impulse responses and emphasis on phase transitions respectively^{76,77}.

For the purpose of demonstrating that multiple oscillators are operating at the same phase and frequency, or that one has become “entrained” on the other, the phase differences may be quantified in a single metric by calculating their coherence, defined as the normalized correlation between their power spectrums, or by a number of algorithms developed to find instances of phase locking. Examples include pairwise-comparisons between individual sources⁷⁸, or short time window-based methods for irregular signals⁷⁹, although the exact perimeters and thresholds for considering signals phase locked may differ.

Neural Oscillations and Visual Perception

Apart from their role as central pattern generators and general modulators of locomotive activities^{8,35}, spontaneous oscillations generated by neural circuits have also been found to affect the perception of visual and auditory stimuli near detection thresholds in

humans^{80,81}, and are integral to the perception of motion in the larval zebrafish optic tectum⁸². Up and down states of cortical hyper or hypo-sensitivity may contribute to the detection of weak stimuli by favoring input from a single direction at a time, essentially acting as a directional sweep of attention.

Additionally, the phase and frequency of flashed visual stimuli has been found to persist in the activities of the optic tectum⁸³ and for a very limited period in the telencephalon⁸⁴, a process known as visual entrainment. In storing the temporal pattern of a stimulus for a short time, entrainment may facilitate behaviors in a similar capacity to short-term memory formation⁸³.

4.2 Aim

Recent work in the field of zebrafish neuroethology demonstrating the presence of a neural oscillator in the larval hindbrain and its relevance to behavior^{8,9,85} ignited my interest in determining whether the oscillations of the telencephalon were part of this same circuit, or related to other processes driving perception and behavior. To this end, I sought to examine both the ways in which external stimuli could affect the dynamics of these oscillations, and how manipulations of the activities of pallial neurons themselves could affect other brain regions.

4.3 Materials and Methods

Pharmacological Manipulation of Spontaneous Activity

For the first set of experiments involving baclofen, two 5DPF larvae expressing gSAIzGFFM119B;UAS:GCaMP6s in a nacre background were immobilized in a 2% low melting agarose solution, covered in E3 buffer, and imaged for spontaneous telencephalon activity under a confocal microscope as described previously. The E3 buffer was then washed out with a 10 μ M solution of baclofen in E3, and left for 30 minutes. After the baclofen bath, the immobilized larvae were washed with E3 buffer again, and reimaged in the same fashion.

The subsequent experiments with baclofen employed a revised protocol, using the maximum concentration found in the previous literature for use in larval zebrafish⁸⁶. Two larvae were imaged as before in the pre-exposure condition, but were treated with a 50 μ M solution of baclofen in E3 for 1 hour before the second round of imaging, and remained covered with the baclofen solution during imaging.

Visual Entrainment Protocol

5DPF larvae expressing gSAIzGFFM119B;UAS:GCaMP6s in a nacre background were fixed in 2% low melting agarose, and covered with E3 buffer. Agarose surrounding the eyes and tails of the larvae were removed as described in the previous closed loop experimental protocols, and the surrounding 60 mm. Petri dish was tilted to align the surfaces of the telencephalon and optic tectum of the larvae for simultaneous imaging under a confocal microscope. 11 larvae were used in pilot experiments to optimize the perimeters of the visual stimulus protocol, and eight larvae were recorded under the finalized stimulus protocol.

Visual stimuli were generated by a custom script using the Psychophysics Toolbox 3 for Matlab⁸⁷. Stimuli were presented to the larvae through a projector with a planar convex lens and a 610 nm. longpass emission filter, with a rear projection screen film directly below the larvae, attached to the bottom of the dish. The protocol for the visual stimulus consisted of constant illumination, with 0.5 second long dark flashes alternating on either side of the larvae at 4.5 second intervals, forming a 10 second cycle of alternating dark flashes that was repeated for 2.5 minutes. After the initial alternating dark flash stimulus, the larvae were presented with an additional 2.5 minutes of constant illumination. A pulse from a National Instruments DAQ device triggered by the stimuli script synchronized the start of the confocal imaging with the onset of the visual stimuli.

Spontaneous/Evoked/Entrained Activity Assay

Larvae were prepared similarly to the previous protocol, with the addition of a 2.5 minute long habituation period prior to the imaging, during which the larvae were presented with constant illumination of the same intensity used in the rest of the experiment, along with the excitation light used for the confocal imaging. Throughout the experiment, the central pixels immediately below the fish along the body axis, extending 5 pixels on each side, were kept at a consistent grey (0.5 level of intensity) to reduce the possibility of unintended visual stimuli from reaching the contralateral eye. Imaging of spontaneous activity began after this habituation period, and continued for 2.5 minutes, followed by 2.5 minutes of visual stimuli and constant illumination, as described in the visual entrainment protocol.

Linear Models and Average Activity per Period

For the linear models, predictors were convolved with an exponential decay function with a 1 second half-life, as per the published kinematics of GCaMP6s⁸⁸, and orthonormalized for the purpose of linear regression⁸⁹.

In all entrainment experiments, cells from the left and right hemispheres of the telencephalon and optic tectum were manually identified and sorted for each optical layer. To remove movement related artifacts from the activity averages, the raw calcium imaging videos were reanalyzed to find the correlation coefficient between each set of successive frames. After normalization to unit variance, frame transitions that dropped below 5 standard deviations of the mean correlation were considered to be part of a movement bout, either from lateral motions inducing rotations or blurs, or by shifts in the z-axis that could not be compensated for by registration. During the periodic segmentation process, periods containing one or more movement bouts were excluded from the average.

Activity Consistency Thresholding

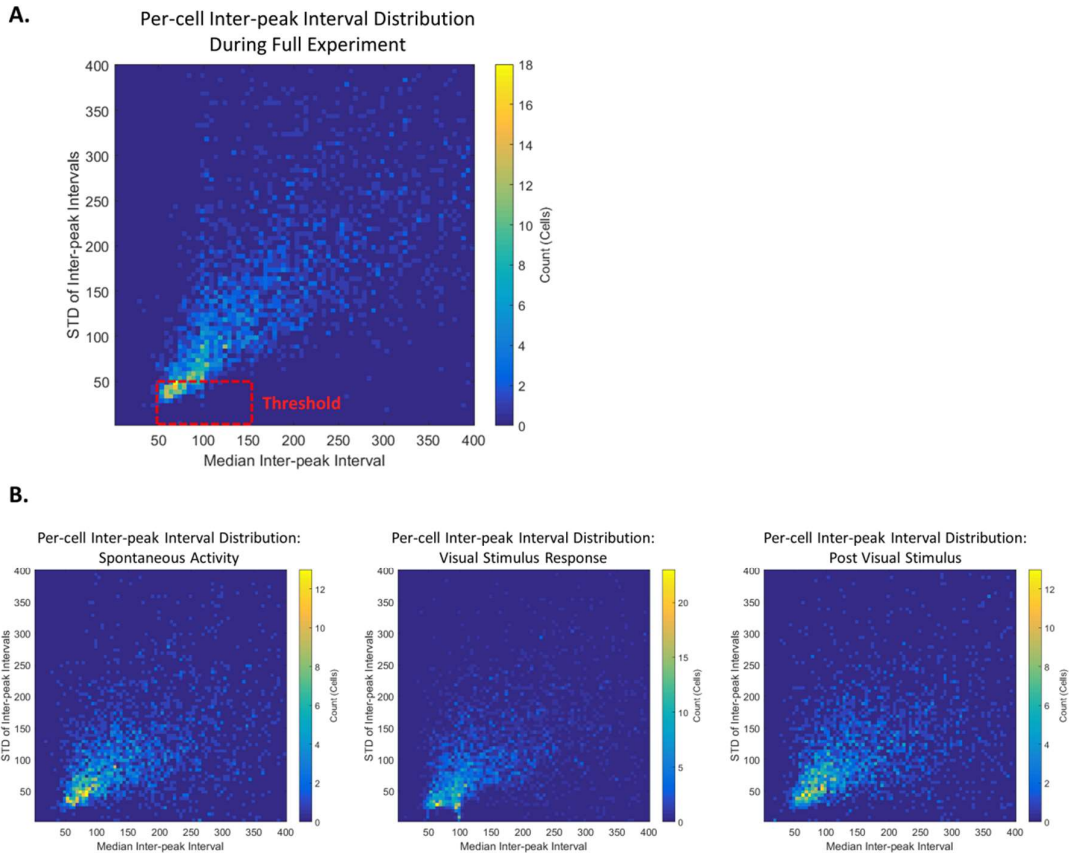


Figure 9: Distributions of Inter-peak Intervals **A:** Density map of cells ($n=5594$) from 8 fish, displayed according to median values and standard deviations of intervals during the entire recording session. The 0.1 Hz periodicity threshold is shown by a red outline. **B:** Density maps of same cells as in 8.A, but medians and standard deviations are calculated for peaks occurring within the 3 separate time periods of the visual entrainment protocol.

For the purpose of narrowing down the analysis to cells with sufficiently high levels of periodic activity, thresholding was performed based on the distributions of inter-peak intervals for individual cells, with cells exhibiting median inter-peak intervals within the range of 50-150 frames and standard deviations lower than 50 frames being selected as meeting the

selection criteria for 0.1 Hz activity (Fig. 9.A). The 0.2 Hz threshold included medians between 40-60 frames, and standard deviations below 50.

Separate statistics for inter-peak intervals occurring during the periods of spontaneous activity, visual stimuli, and post-stimuli were calculated, and cells were sorted into categories based on their particular combinations of active periods.

Phase Analysis

The phase angles of periodic cells were determined by fitting positively rectified 0.1 Hz sine functions that had been convolved with a GCaMP6s decay kernel. Circular means were calculated for phase angles from cells in each anatomical area for each recording session using the CircStat toolbox⁹⁰.

4.4 Results

Baclofen Treatment Reduces Spontaneous Activity

When I treated 5 DPF larvae with a 50 μ M solution of baclofen for 1 hour, they exhibited a reduction in inter-peak intervals in the 50-100 frame range, corresponding to frequencies of 0.1-0.2 Hz (Figure 10). A 30 minute exposure with a 10 μ M solution, however, did not produce a significant change in the distribution of intervals.

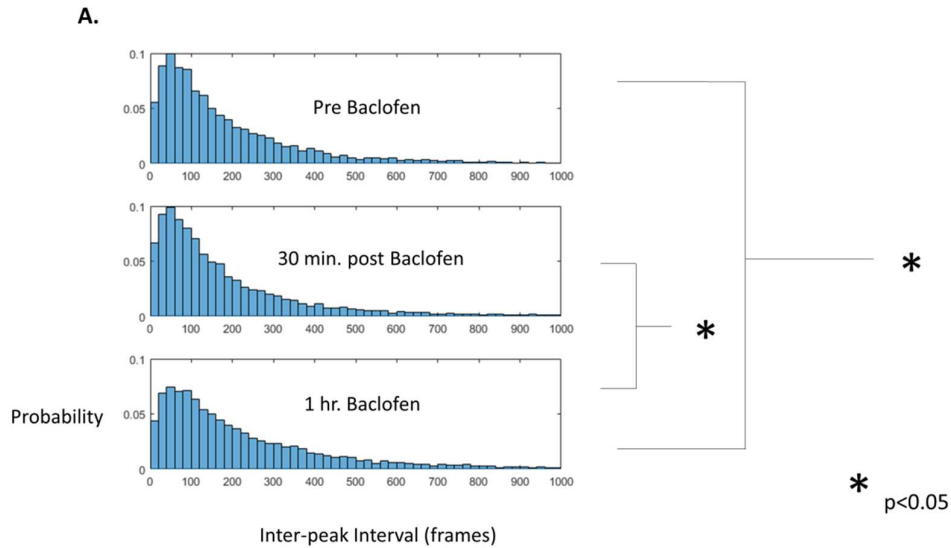


Figure 10: Distribution of Spontaneous Activities after Baclofen Treatment A: Histograms of inter-peak intervals for spontaneous telencephalon activity after 3 treatment conditions. Comparisons between distributions were made by Mann-Whitney U tests. (N= 9551, 15739, and 19070 intervals from sets of 918, 1562, and 2730 cells respectively).

Visual Stimuli-based Entrainment of Telencephalon Activity

Unlike the phase-shifted oscillations observed during the spontaneous activity of the telencephalon which alternated between the left and right hemispheres, responses during and immediately after visual stimuli tended to be bilateral (Figure 11.B). Additionally, I observed peaks of activity in both hemispheres of the telencephalon after stimuli from both the left and right sides of the visual field, as opposed to responses in the optic tectum, which occurred in response to contralateral eye stimulus as expected. Post-stimulus responses of the telencephalon were less consistent, but tended to resemble the visual stimulus responses in terms of phase.

In general, responses to visual stimuli in both the optic tectum and telencephalon were better modeled by a convolved sine function response, rather than a step response, or on-off/off-on impulse responses, with higher ranges of z-scores (Figure 10.C).

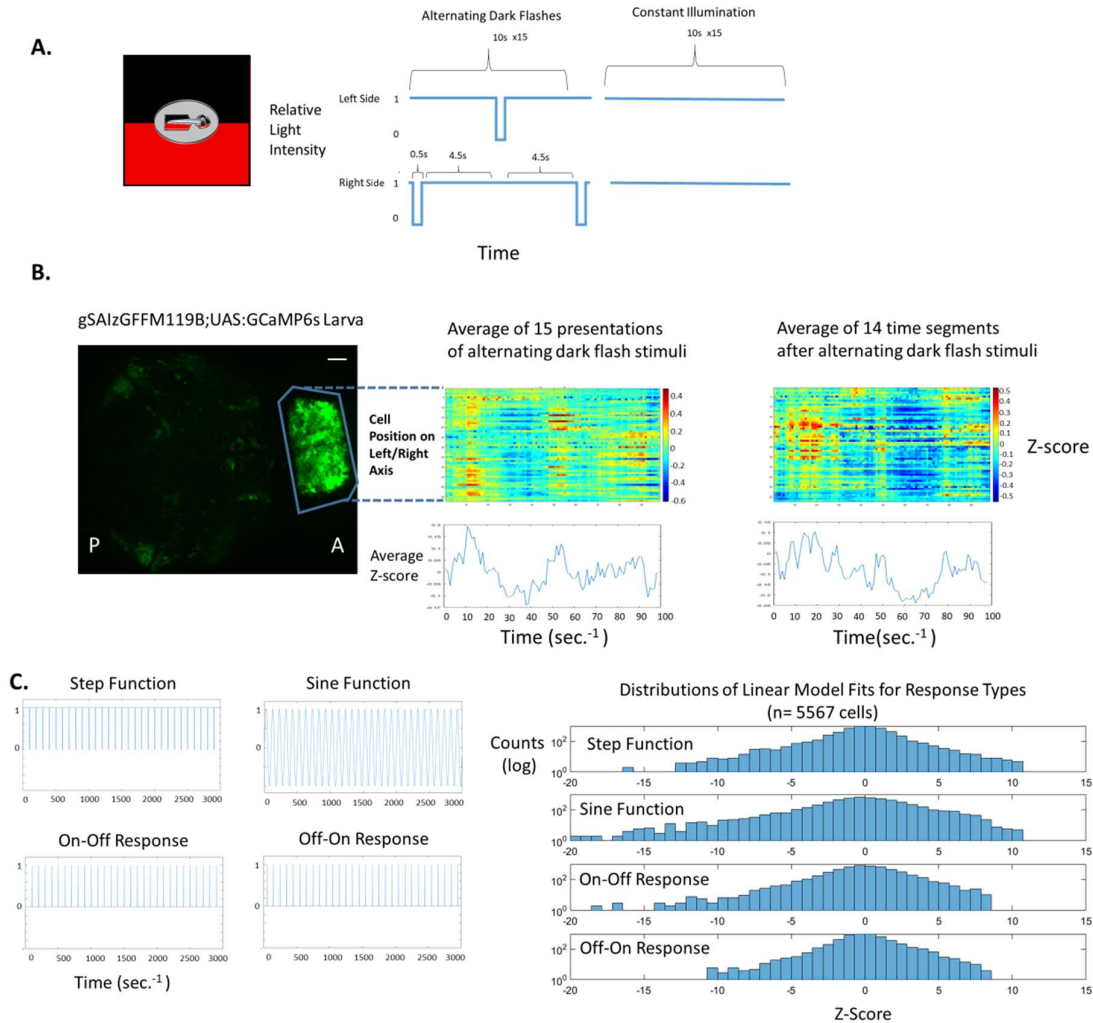


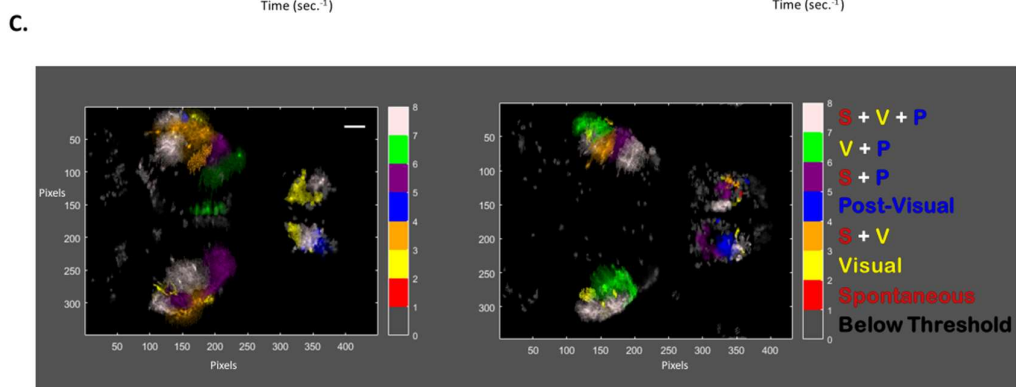
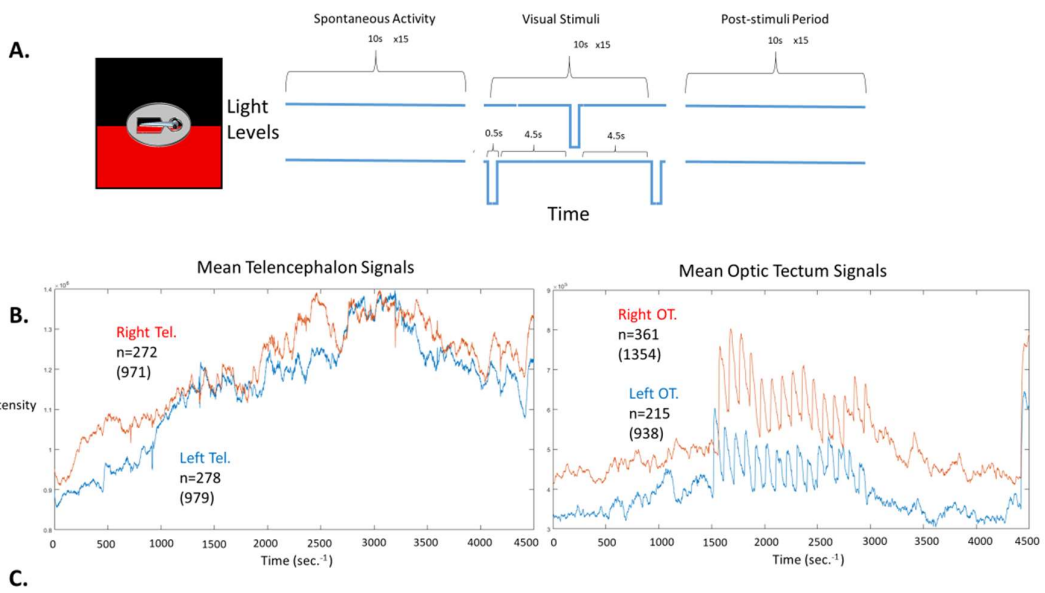
Figure 11: Visual Stimulus-Based Entrainment Assay, Linear Models of Responses **A:** Schematic of visual stimulus protocol. 15 presentations of left/right alternating dark flashes are followed by constant illumination for the same period of time. **B:** Periodic averages of telencephalon cell activities during and after visual stimuli from example recording. Rows are arranged by cell centroid position on left/right axis. Scale bars represent 40 μm . **C:** (Left)

Patterns of possible response dynamics used as regressors in a linear model, prior to convolution and orthonormalization. (Right) Distributions of z-scores for cell signals from 4 fish during visual stimuli regressed against each response pattern.

Ongoing Spontaneous Activity and Visual Entrainment

In an entrainment protocol that was expanded to include recordings of spontaneous activity immediately prior to the onset of alternating dark flash visual stimuli, cells in both the telencephalon and optic tectum exhibited periodic activities before and after the stimulus period (Figure 12.B-C). Additionally, subpopulations showing consistent periodic activity at 0.1 Hz during different sections of the protocol, before, during, and after the presentation of stimuli, but generally symmetric in both hemispheres of the optic tectum and telencephalon. While a significantly greater percentage of tectal cells were active at 0.1 Hz in response to visual stimuli, a greater portion of cells in the telencephalon met periodicity criteria after the visual stimulus ended (Figure 12.D). The particular Gal4 line that was used in the experiments also labeled a sparse population of cells in the hindbrain, although these cells did not meet the periodicity criteria during the course of the protocol (Figure 12.C).

One activity category consisting of cells that displayed 0.1 Hz activities before and after the presentation of visual stimuli but not during the stimulus period itself, denoted as “S+P” cells, contained a subpopulation of cells that did not meet the criteria for consistent 0.1 Hz activity during the visual stimulus period due to oscillating at a consistent rate of 0.2 Hz, with a phase matching the presentation of dark flashes from both left and right eyes (Figure 13.A). While a lower number of cells met the criteria for 0.2 Hz oscillations, the majority of cells responding at 0.2 Hz during the visual stimuli and post-stimuli periods resided in the telencephalon, particularly in posterior and ventral portions of the pallium (Figure 13.B).



D.

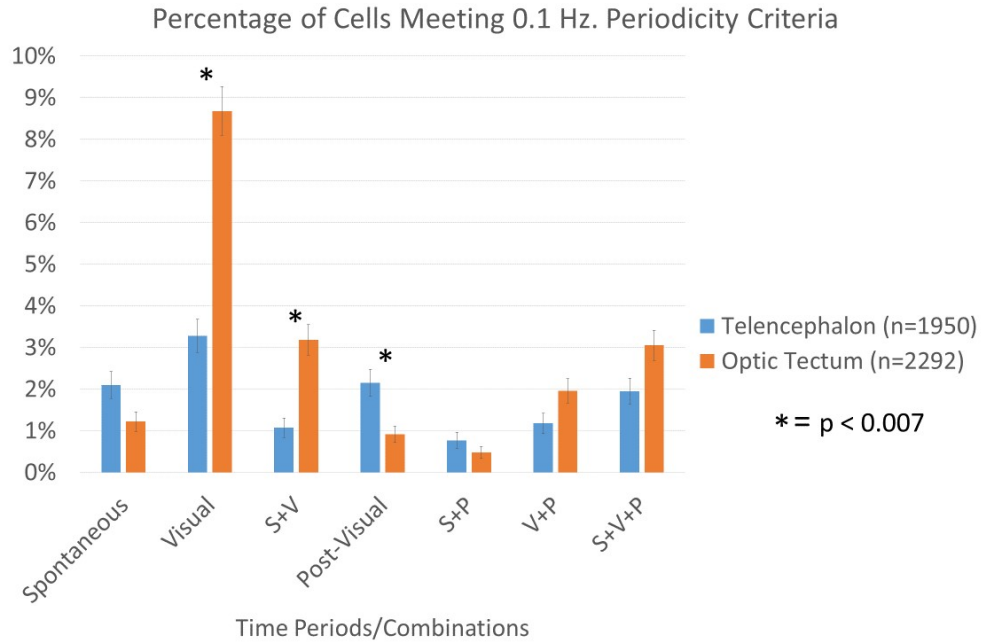
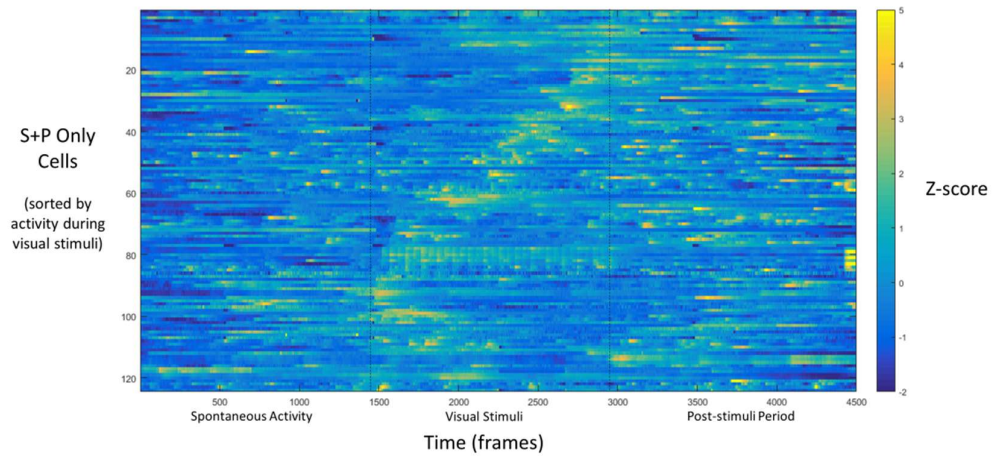
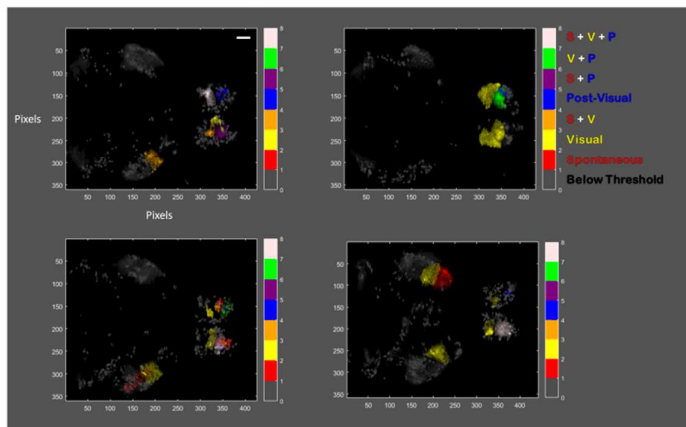


Figure 12: Spontaneous and Visually Evoked Activity A: Schematic of visual stimulus protocol. 2.5 minutes of constant illumination are followed by left/right alternating dark flash stimuli, and then an additional 2.5 minutes of illumination. **B:** Average $\Delta F/F$ intensity values for cells meeting periodicity threshold criteria in 4 brain regions. Total number of analyzed cells pre-thresholding are given in parentheses. **C:** Cells from 2 example recordings, colored by combination of time periods in which each cell met the 0.1 Hz periodicity criteria. Scale bars represent 40 μm . **D:** Percentages of cells in each ROI set (Telencephalon and Optic Tectum) from all fish, meeting the 0.1 Hz periodicity criteria during particular time periods and combinations thereof. Bars show standard errors.

A. Activities of Cells Meeting 0.1 Hz. Criteria During Spontaneous and Post-Visual Periods Only



B. ROIs of Cells Meeting 0.2 Hz. Criteria



C.

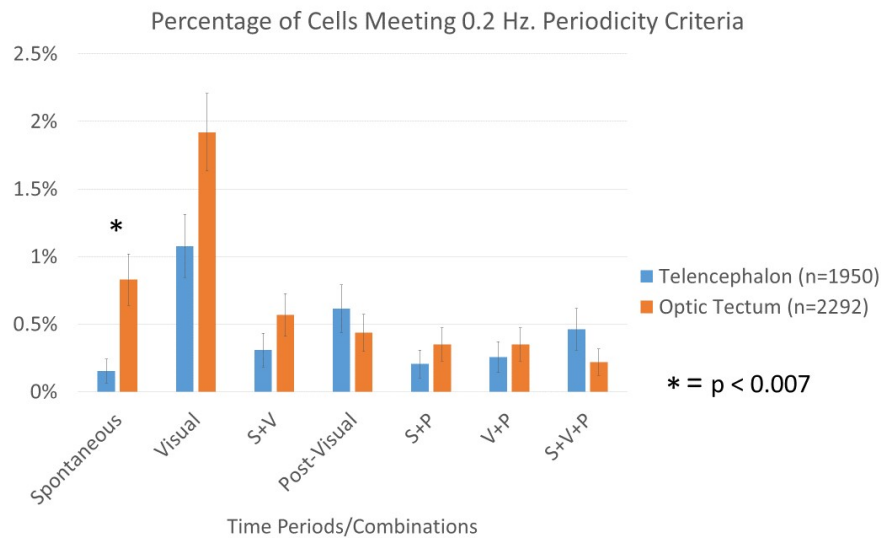


Figure 13: 0.2 Hz Oscillations During Visual Stimuli: Heatmap of calcium activities for cells that met the 0.1 Hz periodicity criteria as in Figure 9 during the spontaneous and post visual stimuli portions of the visual stimulus protocol (“S+P” Cells), but not during the presentation of alternating dark flashes. **B:** Cells from 4 example recordings, colored by combination of time periods in which each cell met a 0.2 Hz periodicity criteria. Scale bars represent 40 μm . **C:** Percentages of cells in each ROI set (Telencephalon and Optic Tectum) from all fish, meeting the 0.1 Hz periodicity criteria during particular time periods and combinations thereof. Bars show standard errors for ANOVA comparisons of telencephalon and optic tectum activity categories.

4.5 Discussion

On Pharmacological Experiments

In the experiments with baclofen treatment, I only found a significant effect on the rates of spontaneous activity with high dosages and exposure times greater than 1 hour. As the mechanism of action for baclofen involves the binding of G protein-coupled GABA_B receptors, the onset of its effect can be expected to be slower than that of drugs targeting GABA_AR⁸⁶. However, the experiments were unsuccessful in uncovering the possible role of mutually inhibitory interneurons in the maintenance of the alternating oscillations of the telencephalon. In further explorations on the effects of pharmacological interventions on spontaneous activity, it will be necessary to establish the effects of GABA antagonists, as well as the minimal dosage of GABA agonists required for visible changes in frequency content, as it is possible that the dosages used in the present experiments produced a degree of silencing that precluded the possibility of any more subtle changes in the phase relations between the two hemispheres.

On Visual Entrainment

In the revised protocol for visual entrainment, it is likely that the addition of a 2.5 minute habituation period prior to the spontaneous imaging was not sufficient to acclimate the larvae to the light produced by the projector, as the average levels of activity in both the telencephalon and optic tectum increased over the course of the 2.5 minute spontaneous activity imaging period (Figure 12.B). Additionally, future versions of this experimental setup may be better served by the use of 2-photon imaging, rather than confocal, as the

excitation light used in the imaging was possibly disruptive to the contrast of the projected stimuli below the larvae.

One additional point of interest to note is that responses to left/right alternating dark flashes in both the optic tectum and telencephalon showed higher ranges of z-scores, indicating better levels of fit⁸⁹, when regressed against a sinusoidal function, rather than for functions based on tonic responses to light intensity, or on-off responses, even though all of the functions were convolved to match the slow dynamics of GCaMP6s signals (Figure 11.C). This is particularly surprising given the short duration of the presented stimulus, which was only 0.5 seconds for each side, relative to the length of each cycle. Because this prolonged response may be the result of an integration of light intensity signals, it is worth checking if the linear model would be better served by the use of convolved triangle waves, which would be the integral of the square wave function expected from direct responses to stimulus intensity. However, distinguishing the subtle differences between the two response functions may require further experiments using dark flash durations of different lengths to check if the linear regression scores diverge.

While the phases of the active cells, both in their responses to visual stimuli and the phases of their activities during the post-stimulus period, play a large role in the overall story of this chapter, the phase-fitting methodology produced spurious results when used with the spontaneous activities of individual cells acting as negative controls. The data appears to suggest that telencephalic cells may respond to either left or right eye stimuli depending on the phase of their earlier spontaneous oscillations (Figure 17.C), and retain population activities that are phase-locked during the post-stimulus period (Figure 17.D). However, these data are discussed further in chapter 6.2, as an area in need of further improvement, as the results are not yet confirmed by an alternative phase-fitting method.

Possible Models

The largest question raised by the results of this chapter is the mechanism behind the sudden switch from alternating to bilateral patterns of activity with the addition of visual stimuli. Lines of evidence that may point to particular models include the abundance of cells exhibiting 0.2 Hz activities, phase locked to stimulus from both eyes. While a portion of these cells responding to stimuli in a bilateral manner belonged to cells and regions of neuropil, as expected from previous results involving the computation of bilateral visual motion stimuli in whole-brain recordings²⁰, although the majority of the cells identified in my experiments that were responsive to alternating dark flash stimuli in a bilateral fashion resided in the posterior and ventral pallium of the telencephalon. Also notable was the lack of a bilateral response from cells in the cerebellum and other hind-brain areas, which have been described extensively in larval zebrafish studies of putative oculomotor integrators^{91,92}, although the comparatively sparse labeling of hindbrain neurons in the Gal4 line used could be an explanation for this discrepancy.

One possibility for a mechanism behind the shift to correlated activities in the telencephalic oscillator is bilateral input from either hemisphere of the optic tectum to both the left and right hemispheres of the telencephalon, overpowering the mutual inhibition that would otherwise produce alternating oscillations. A similar model, containing both mutual inhibition and bilateral feedforward input from visual centers has been proposed to account for the effect of visual feedback on the phase of the ARTR, although in the case of that circuit, only simultaneous flash stimuli from the left and right eyes was capable of decreasing the average phase angle difference between the left and right hemispheres, and did not fully disrupt the anticorrelation of their activity patterns⁹.

An additional source of information valuable to the creation of a model for the functional connections in the larval zebrafish telencephalon are anatomical databases for larval zebrafish brains that contain copious amounts of information on the cell types present in day 5-6 larvae, integrating imaging stacks of immunohistochemical stains and fish lines with tags for genes associated with particular neurotransmitter receptors^{40,68}. At day 6 of development, the dorsal surface of the pallium is tagged by Vglut2a-GPF, as are a portion of cell bodies within the optic tectum, and the remainder of pallial neurons are positive for anti-TH staining⁴⁰, suggesting a primarily catecholaminergic population surrounded by glutamatergic cells, both of which could conceivably account for the levels of self-excitation in each hemisphere necessary for maintaining ongoing spontaneous activity. The subpallium and anterior commissure at this stage, in addition to a majority of cell somas in the optic tectum, are strongly tagged by Gad1b-GPF⁴⁰, providing suitable candidates for the necessary mutually inhibitory projections expected in an oscillating neural circuit. Projections to the pallium or subpallium carrying visual information, or ascending signals associated with processed visual cues, are another vital piece of the model in order to explain the phase-locked response of pallial cells to dark flash stimuli. In zebrafish larvae around the 4 day stage, the presence of ascending dopaminergic and noradrenergic projections from the diencephalon and hindbrain to the subpallium and pallium may account for the indirect transmission of phase information from visual inputs^{7,93}.

Chapter 5: Closed Loop System for Larval 2D

Navigation

5.1 Background

Behavioral Repertoire of Zebrafish Larvae

Owing to the fast development of zebrafish larvae, a number of visually driven behaviors can be observed as early as 3 days post-fertilization, such as the tracking of rotational motion (the OKR, or optokinetic response)⁹⁴, prey tracking and capture behavior as soon as day 4 of development⁹⁵, and compensation for perceived background motion (known as the OMR, or optomotor response) at day 5⁹⁶.

In addition to these well described visually driven behaviors, zebrafish larvae have been observed to perform behaviors rooted in ongoing internal processes, such as biases in turning direction which are related to periodic slow oscillations in a subpopulation of hindbrain neurons⁸, or the initiation of swim bouts, which are driven by stochastic processes that can be modulated by visual input⁹⁷.

Memory dependent tasks, such as associative or spatial learning, are likely to require the telencephalon, as shown by ablation experiments in other teleosts¹¹. However, studies of classical and operant conditioning in zebrafish over the course of development have only managed to successfully demonstrate learning in fish as young as 3 weeks⁹⁸, although habituation to touch stimuli and entrainment of visual stimuli have been demonstrated in larvae younger than 1 week^{69,83,99}.

Closed Loop Behavioral Assays

In the field of neuroethology, virtual reality experiments, or closed loop behavioral assays have rapidly come into prominence as a technique for observing neural activities in behaving animal subjects, since the head of the animal can be fixed in place as it navigates a virtual environment. In mouse studies, rotatable spheres are used both as a support for the animal, as well as a means to track changes in position through optical sensors monitoring rotation of the sphere on several axes¹⁰⁰.

Zebrafish pose a unique challenge in terms of virtual reality setups, in that their fictive motions must be inferred indirectly, since the trackball approach is not feasible. Previously, zebrafish researchers have approached this problem by optically tracking the tails of head-fixed larva, or measuring electrical activity at the neuromuscular junction of muscles in the tail of paralyzed larvae^{85,101,102}. In a paper describing an optical approach, a position-sensitive device was used to measure the onset of motion in a binary, on/off fashion, and the stimulus position was updated to a predetermined position rather than being determined by the particular dynamics of the fish's movements due to latency concerns¹⁰¹.

Closed loop systems with integrated calcium imaging using paralyzed larvae have previously been demonstrated for 1-dimensional optomotor response assays⁸⁵, and 2-dimensional navigation assays¹⁰². In an optomotor response assay, reflexive movement is induced by whole field motion, normally taking the form of stripes constantly moving rostral to caudally with respect to the fish as a stimulus, resulting in bouts of forward swim movements by the fish to compensate for a perceived backwards movement. In the closed loop system developed by Ahrens et. al., the gain of this forward movement could be altered in order to examine forebrain and hindbrain regions involved in the modulation of the response⁸⁵. Virtual behavioral assays offer the ability to easily alter environmental parameters

during testing, including parameters that would otherwise be fixed, such as the rate at which the animal moves through its environment.

Employing the same principle of recording muscle impulses in paralyzed larvae, Ahrens et. al. later created a closed loop 2D navigation assay by measuring the comparative strengths of signals from neuromuscular junctions in the left and right halves of larval tails¹⁰². In the assay, the fixed larvae were capable of replicating behaviors observed in freely swimming larvae, such as turns in response to angled optomotor stimuli, and phototaxis exhibited by avoidance of dark portions in a 2D environment during a virtual navigation assay.

One important factor to note regarding paralyzed larvae setups involves the use of α -bungarotoxin to paralyze the larvae, which affects nicotinic acetylcholine receptors at the neuromuscular junction in skeletal muscles. However, α -bungarotoxin also acts upon a range of different nicotinic acetylcholine receptors, including $\alpha 7$ receptors in interneurons, possibly affecting behavioral results¹⁰². In adult zebrafish, selective antagonists for $\alpha 7$ were shown to reduce performance in t-maze tests, indicating that blocking these receptors may affect memory and spatial learning¹⁰³.

In 2016, after the experiments described in this chapter were performed, a separate research group published a paper describing a similar closed loop 2D navigation system for larval zebrafish based on optical tail tracking¹⁰⁴. This system, however, did not include a means of recording neural activity during behavioral assays.

5.2 Aim

In attempting to find a relationship between the oscillatory activities of the telencephalon and eventual behavioral outputs, I realized the necessity of a system allowing for calcium imaging to be performed in behaving larvae. To simplify the process of preparing larvae for the closed-loop system, I decided to use image tracking to measure tail movements during fictive swims, rather than making electrophysiological recordings of motor neurons in paralyzed larvae. While the current system did not achieve reliable tail motion tracking when incorporated into an imaging setup, further optimizations could provide a platform for behavioral experiments in non-paralyzed larvae.

5.3 Materials and Methods

Closed Loop Assay Setup and Behavioral Protocol

5-6 day old UT or nacre larvae were placed in 3ml. of 2% low melting agarose on a 60 mm. diameter plate, and covered with E3 buffer solution once the agarose had set. Portions of the agarose surrounding the tail, up to the swim bladder of the larvae were cut away with a microscalpel, as well as the agarose surrounding the eyes of the larva, allowing for free movement of the tail and eyes. The fixed larva were then placed on a 162.05 mm. x 121.54 mm. LCD screen with a 1024 x 768 pixel resolution, and a circular array of infrared LEDs were positioned 2 cm. above the larvae for lighting. A XIMEA MQ013RG-E2 near-infrared camera was used with an optical microscope at 2x magnification to record larval tail movements at approximately 60 frames per second (Figure 14. A). Prior to each experiment, the user selected a rectangular region perpendicular to the body axis of the larva, covering the end-most third of the larva's tail. The position of the intensity weighted centroid on the

vertical axis of this region was recorded, representing the vertical movement of the tail of the larvae (Figure 14. C). At each frame, a moving 320 millisecond window of previous tail movement was taken, and a single-sided amplitude spectrum for the tail movement was created via a Fourier transform (Figure 14. E). The amplitudes of two portions of the spectrum, 3-5 Hz and 25-30 Hz, were then averaged. These slow and fast frequency components, correlating with turn movements and forward swims in free moving larvae¹⁰¹ were then used to update the angle of rotation and translation of the displayed background respectively. A 10% smoothing factor was also added between frames to simulate inertia¹⁰², along with constants that were subtracted from the velocity at each frame, simulating friction and water resistance. During the closed loop experiments, display updates were drawn at 30 frames per second, leading to an inherent latency of 32 milliseconds between tail movements and movement of the virtual environment. The angle and position of the fish in the virtual space were recorded and time-stamped for each captured frame, along with the tracked tail position.

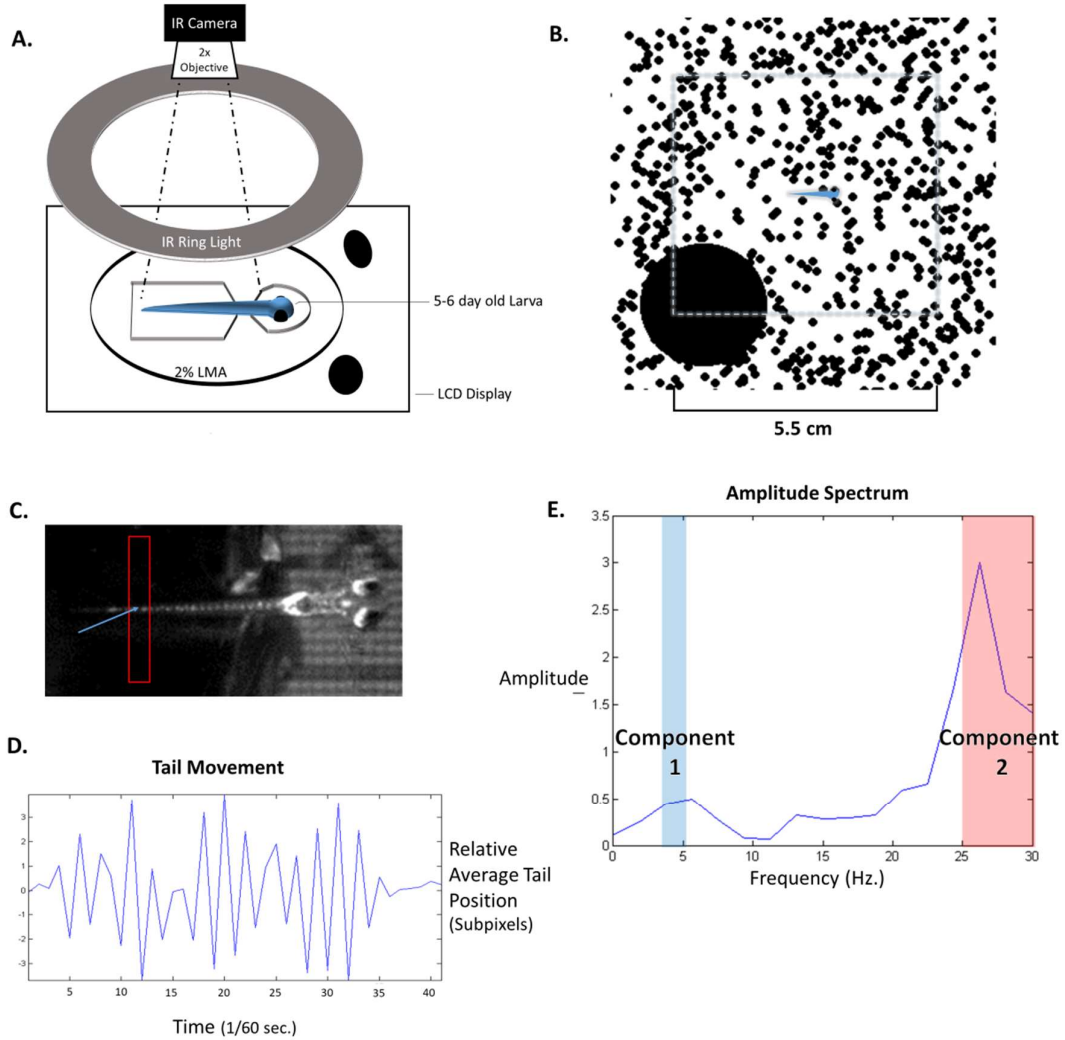


Figure 14. Closed Loop System. **A:** Diagram of the closed loop system set-up. **B:** High-contrast environment of small (6-px. diameter) and large (99-px. diameter) dots. The portion displayed on screen (5.5 cm²) is shown by the dotted line. **C:** A rectangular region of interest (red), with the averaged point of highest intensity on the vertical axis shown with a blue arrow. **D:** Tail position, as measured by the criteria of 3.C, over the course of one swim bout. (Approx. 0.67 seconds) **E:** Single-sided amplitude spectrum of the first 20 frames of 3.D (0.33 seconds), with a slow frequency component (3-5 Hz) highlighted in blue, and a fast frequency component (25-30 Hz) highlighted in red. In the closed loop system, the average of

component 1 and the average of component 2 are used to update the rotation and the translation of the background displayed to the fish, respectively.

Optimization of Simulation Parameters

A free swimming 5 DPF larva was imaged under a dissecting microscope with 10x magnification at 60 frames per second. A single contiguous segment of video lasting 11.2 seconds was used in further analysis, containing 6 bouts of movement during which the entire larvae was visible in frame (Figure 15.A) The video of the moving larva was then registered to the initial frame, aligning the head in each frame in order to create a virtually fixed larva with visible tail motion and a known intended path, calculated as the movement with respect to the central point on the swim bladder of the larva, with turns as a rotation around this point (Figure 15.A Right).

Tail movements measured from the video of the virtually fixed larvae could then be used in lieu of live video in the closed loop system, with the resultant virtual movement path as output (Figure 15.B). The sum of the squared errors between points in this virtual movement path and the actual path of the free swimming larvae was then used as a cost function in the optimization of the parameters controlling movement scaling factors in the virtual environment, which was accomplished through simulated annealing using a stochastic sampling method¹⁰⁵.

With the parameters of the closed loop system set in place, the effect of the precise placement of the ROI on the accuracy of the predicted movement could be tested using the same scheme. Rectangular ROIs with widths between 1 and 30 pixels were placed at starting

points spanning 150 pixels across the length of the larva's tail, and error scores were generated for each configuration (Figure 15.C).

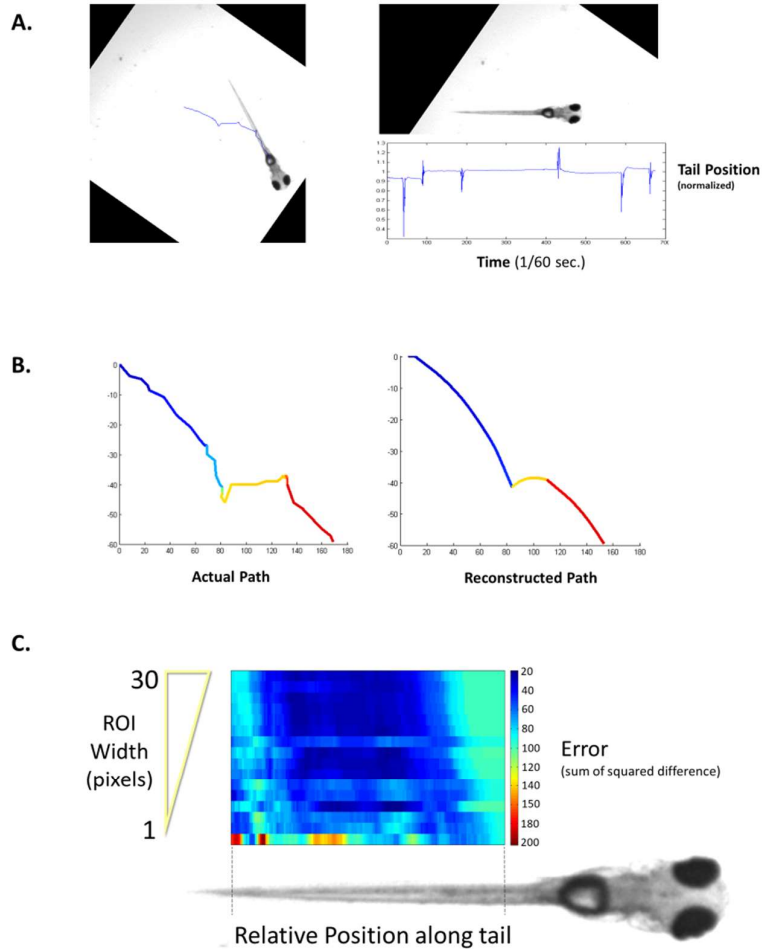


Figure 15. Optimization of Virtual Reality Parameters. **A:** (Left) Path of larva during multiple swim bouts, shown as a blue line. (Right, top) First frame of video fixed relative to position of larva (Right, bottom) Tail position over time, calculated from centroid position of tail section in y-axis. **B:** (Left) Path of free swimming larvae, colored from blue to red over time. (Right) Path reconstructed from tail position signal, colored with same schema as left figure. **C:** Accuracy of path reconstruction based on position and width of ROI.

Virtual Reality Navigation Assay

For the 2D avoidance assay, the virtual environment took the form of a looped 300^2 pixel image consisting of randomly spread 6 pixel diameter spots, with a single 100 pixel diameter spot in the lower left corner. A 200^2 pixel portion of the image was displayed to the larvae over a 5.5 cm^2 area, and looped as the larvae made fictive swim movements in the virtual environment (Figure 16. B). In total, 2 larvae were used for analysis in the spot avoidance assay with the parameters described.

5.4 Results

Larvae Show Expected Avoidance Behavior in Closed Loop 2D Navigation System

After 20 minutes of habituation to the closed loop system, 6 day old UT larvae tended to avoid intersecting with the 2.75 cm. diameter spots in the virtual environment. In 2.2 minute trials, the fish exhibited avoidance of the spots that became progressively more accurate (Figure 16.A, B), and exhibited swim paths with lower rates of total rotation (Figure 16.D). Additionally, the frequency of swim bout movements decreased over the course of the trials (Figure 16.C), but total distances moved during the trials remained relatively constant.

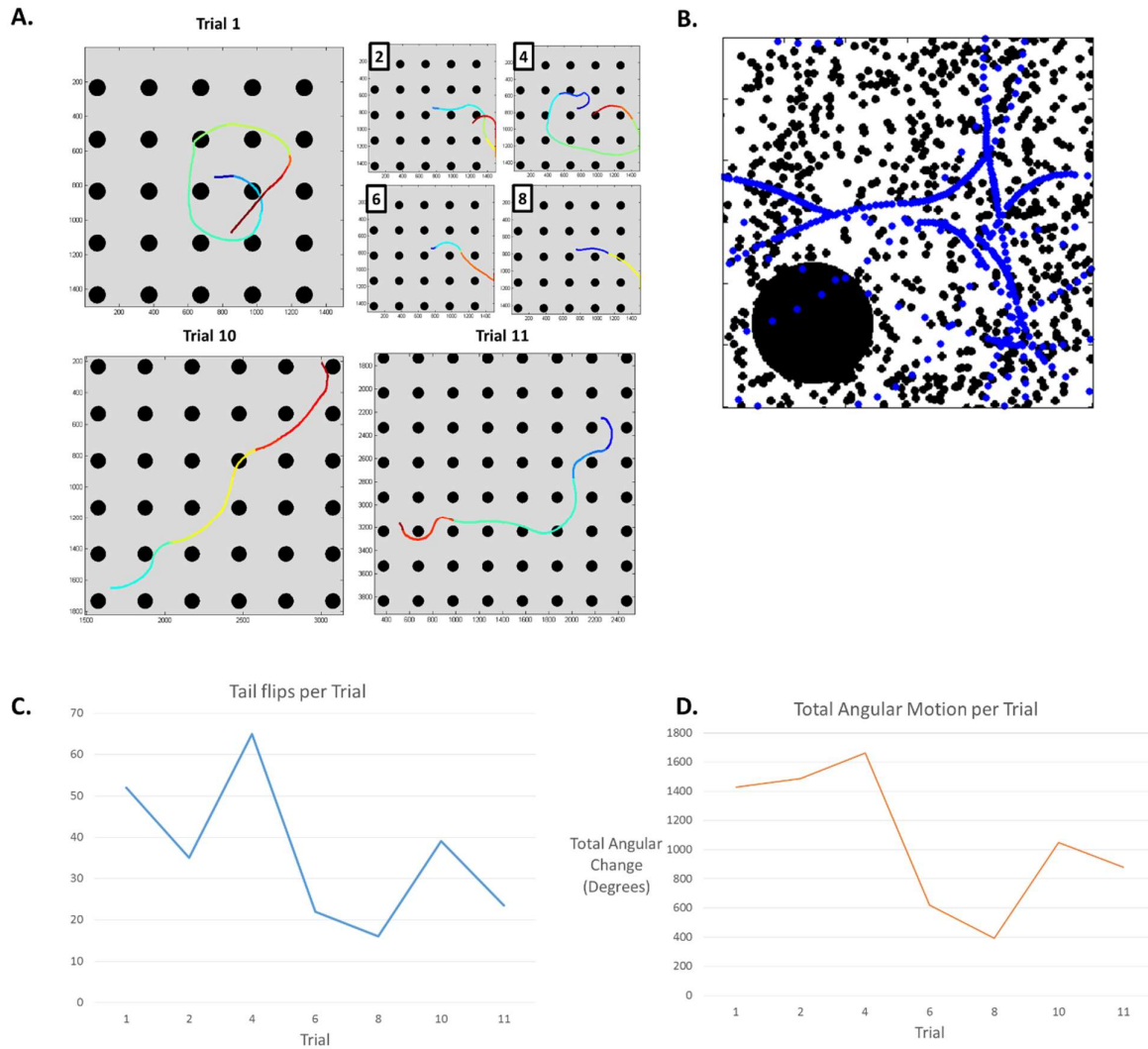


Figure 16. 2D Navigation Assay. **A:** Traces of a single 6 day old, UT larvae over 10 2.2 minute trials, concluding with a single 5 minute trial. For visual clarity, only the large spots in the repeating background are shown. The traces are colored by time, from blue to red, with abrupt changes in color representing points between swimming bouts. **B:** The movement trace (blue) of the larva during trial 11, overlaid upon the repeating tile pattern. **C:** The number of tail flips per trial, defined by the number of peaks in total tail movement that exceeded a value of ± 10 pixels in amplitude. **D:** The cumulative changes in heading angle made by the fish during each trial (in degrees).

5.5 Closed Loop System for Larval 2D Navigation

In the data shown for the closed loop system, the parameters for forward and rotational movement gain, as well as the coefficients for friction, were not optimized based on the movement speeds of freely swimming larvae. Therefore, it is highly likely that the larvae in the closed loop system experienced visual feedback which was interpreted as the environment moving at an unexpected rate. This can be observed directly in the traces of tail movement taken over each trial, as the number of swim events (measured in tail flips) for each larvae decreases over the trial periods (Figure 16.C). Additionally, while the manual placement of ROIs for the purpose of tail tracking was a possible source of experimental error, simulations of alternate ROI placements suggested that the accuracies of path reconstructions were not adversely affected by small differences in ROI position given sufficiently wide ROIs that were able to integrate multiple tail points (Figure 15.C).

Taken in total, these results suggest that the larvae is undergoing motor adaptation based on the visual feedback of the closed loop system, a process which has been shown previously in 1-dimensional closed loop assays⁸⁵. In order to adjust the perceived motion of its environment towards an expected rate of motion, the larvae modulates its motor programs, altering the intensity and frequency of its swimming motions. In the closed loop system, the parameters for the gain of the forward velocity and rotation rate, along with the variables representing friction, were only roughly optimized, resulting in a system that produced a much higher rate of virtual movement than would be normally encountered by free-swimming larvae. Optimizing these parameters may result in shorter habituation times for the larvae, as the virtual motion of the background would provide a finer match for the expected degree of motion.

The greatest limitation of the current closed loop set-up is the lack of integration with an imaging platform, an issue shared with previous methods employing an optical tail tracking approach^{101,104}. While considerable efforts were made to adapt the system for use in conjunction with a confocal microscope, technical issues involving lighting and camera synchronization impeded progress towards this goal. Parts of the system, however, were able to be adapted for use in non-interactive displays of visual stimuli for imaged larvae, which are described in chapter 4. Additionally, while portions of the system are synchronized through the use of DAQ devices, the actual motion-to-photon latency for the system should be described, although previous studies of closed loop systems in larval zebrafish have only found significant behavioral differences when visual stimulus was updated at latencies greater than 50 milliseconds during fictive prey capture events¹⁰¹.

Moving forward, a closed loop system integrating calcium imaging may act as a platform for future experiments involving larval zebrafish navigation on a 2D plane. In particular, studies on spatial memory may be interesting from a research standpoint, as the capacity for spatial memory has been previously demonstrated in adult teleosts¹⁰⁶, but the precise neural mechanism, or whether teleosts possess the equivalent of place or grid cells has yet to be described.

Chapter 6: Conclusion

In this chapter I will briefly summarize the results of the previous sections, detailing my work on the identification and characterization of the spontaneous activities of the larval zebrafish telencephalon, and relating these results to the larger context of the project as a whole. Since the work of this thesis is not yet complete in some areas, a number of questions still remain. I will therefore also include proposals for directions of further research to address each of them.

6.1 Dynamics of spontaneous activity in the larval zebrafish telencephalon

Through analysis of calcium imaging data from neurons in the dorsal pallium of the larval zebrafish at five days post fertilization, I found a population of neurons with periodic activities at approximately 0.1 Hz, alternating between the left and right hemispheres. Curious about the extent and consistency of these oscillations, I began a project to streamline the analysis of calcium imaging videos taken by confocal microscopy, enabling me to gather frequency data at whole-brain scales, and compare a number of different larvae.

By accumulating data at different depths in the telencephalon, I identified a gradient of intrinsic frequencies in spontaneously active cells across the anteroposterior axis of the pallium. These intrinsic frequencies were consistent over long imaging periods, and the trend of higher frequency cells being located more anteriorly was shared across all imaged fish, including larvae at day 6 of development.

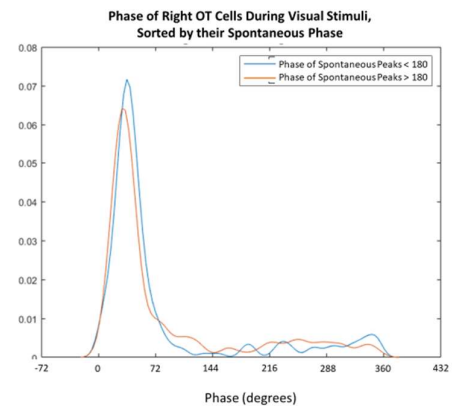
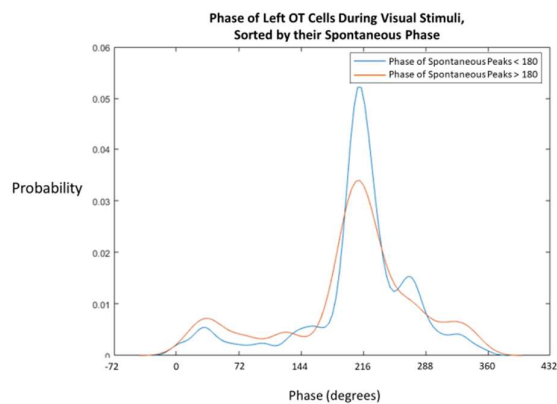
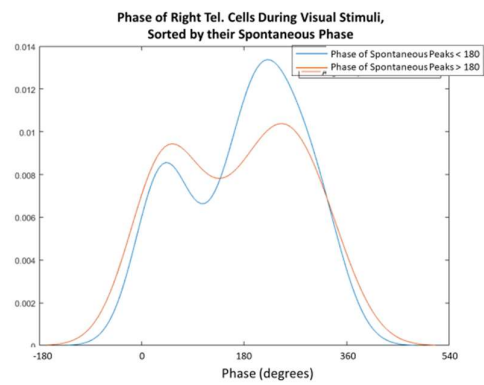
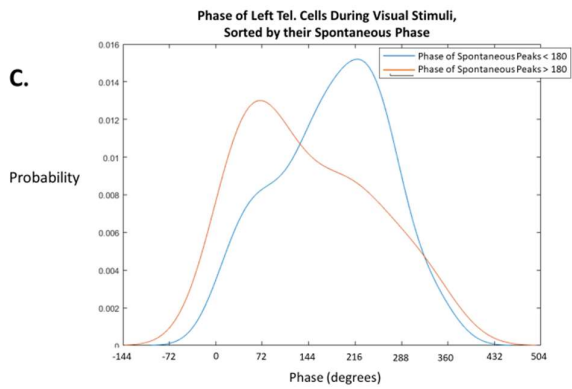
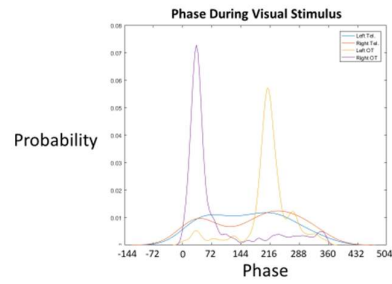
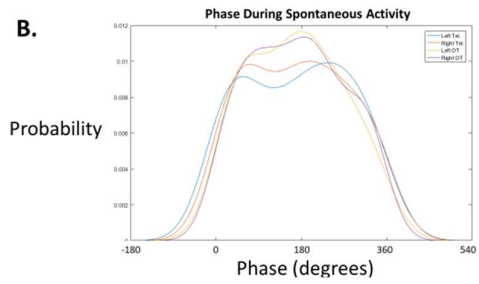
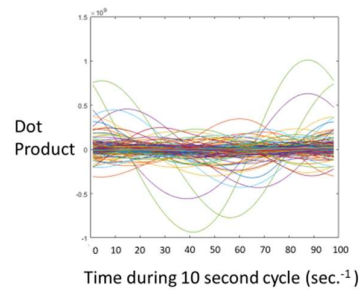
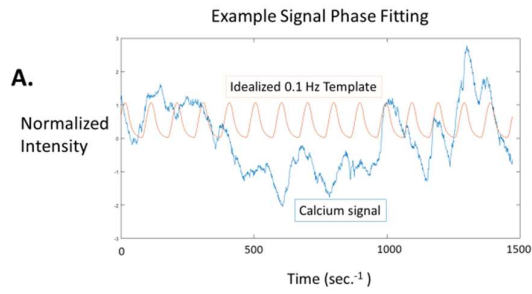
However, the scope of this project did not include the developmental time course of these activities, which would provide vital insight into the origins of this particular pattern of activity. Since the larval zebrafish telencephalon exhibits a defined pallial neuropil as early as 60 hours postfertilization¹², longitudinal studies of its spontaneous activities may be possible,

although great care would be required to establish continuity between cell populations and regions over the course of multiple days, due to the high degree of neural proliferation and migration during these stages.

6.2 Effect of visual input on telencephalon oscillations

In attempting to manipulate the phases of the telencephalon oscillator to further elucidate its mechanics, I found populations of cells in the telencephalon that were both involved in spontaneous oscillations, and responses to visual stimuli. Additionally, when aggregated, these cells appeared to retain the phase of visual stimuli for a short period afterwards (Fig. 17.D), a possible precursor to circuits able to integrate visual information over short time-scales.

Although the results of phase analysis for responses to visual stimuli initially appeared promising, with visual responses in the telencephalon appearing to depend on their initial spontaneous phase (Fig. 17.C), these data were not included in chapter 4 due to unevenly distributed phase angles during the periods of spontaneous activity (17.B), which should ostensibly act as negative controls. As the lighting conditions did not change between the initial habituation period and the onset of recording, the phase of ongoing spontaneous oscillations should in theory be randomly distributed, suggesting a source of bias in the phase fitting methodology.



D.

Per-Trial Average Phase

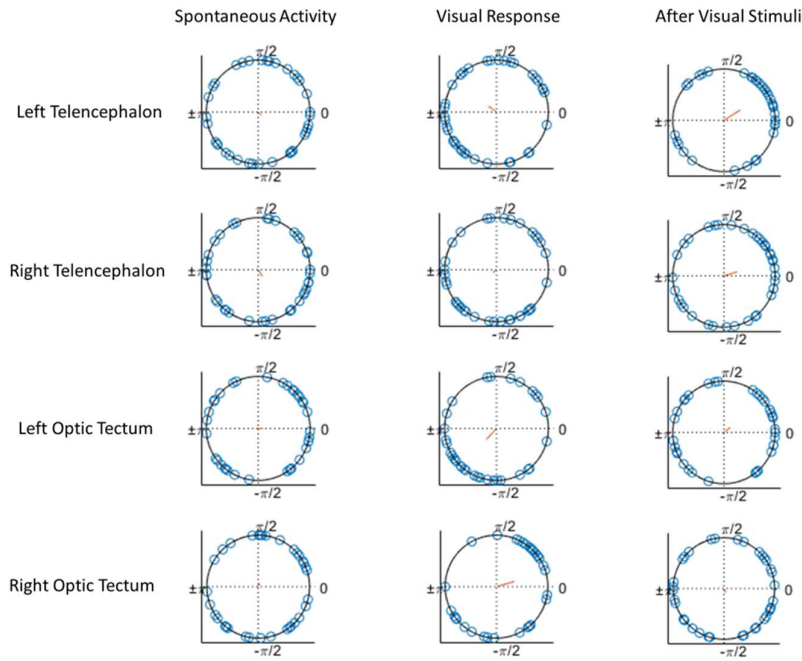


Figure 17. Phase Analysis of Spontaneous and Visually Responsive Cells. A: Illustration of phase fitting method. (Left) Calcium transient from example cell is compared to an idealized GCaMP6s convolved 0.1 Hz response. (Right) Dot products of calcium transients against 0.1 Hz template signals at varying phases. Maximum values are best fits for each phase. **B:** (Left) Probability distributions of phases during spontaneous activity for periodic cells in left and right hemispheres of the telencephalon and optic tectum. (Right) Probability distributions of periodic cells during visual stimuli. **C:** Probability distributions of phase activity in response to visual stimuli, separated by phase of each cell during spontaneous activity. **D:** Circular averages of phases (in radians) for cells in each trial, separated by regions (rows) and time periods (columns). Phases are shown as blue circles, and circular averages of all trials for each region and time are indicated by red lines.

Further analysis with a revised phase fitting method seems warranted, with one candidate being broadband Hilbert transform-based methods for phase analysis⁷⁷, as used in another recent study of oscillatory activities in the larval zebrafish brain⁹.

Acknowledgements

I would like to thank my thesis advisor, Dr. Koichi Kawakami, for his guidance and patience during the course of this project, in regard to the use of genetic engineering techniques with zebrafish larvae. I would also like to thank all of the members of Kawakami lab for their feedback and assistance, particularly Dr. Akira Muto, who instructed me on the basics of calcium imaging and the use microscope equipment. Last of all, I would like to thank the members of my Thesis Committee.

Bibliography

1. van Santen, J. P. H. & Sperling, G. Elaborated Reichardt detectors. *J. Opt. Soc. Am. A* **2**, 300 (1985).
2. Takemura, S. *et al.* A visual motion detection circuit suggested by *Drosophila* connectomics. *Nature* **500**, 175–81 (2013).
3. Korn, H. & Faber, D. S. The Mauthner cell half a century later: a neurobiological model for decision-making? *Neuron* **47**, 13–28 (2005).
4. Friedrich, R. W., Genoud, C. & Wanner, A. A. Analyzing the structure and function of neuronal circuits in zebrafish. *Front. Neural Circuits* **7**, 71 (2013).
5. Temizer, I., Donovan, J. C., Baier, H. & Semmelhack, J. L. A Visual Pathway for Looming-Evoked Escape in Larval Zebrafish. *Curr. Biol.* **25**, 1823–1834 (2015).
6. Chen, X. & Engert, F. Navigational strategies underlying phototaxis in larval zebrafish. *Front. Syst. Neurosci.* **8**, 39 (2014).
7. Tay, T. L., Ronneberger, O., Ryu, S., Nitschke, R. & Driever, W. Comprehensive catecholaminergic projectome analysis reveals single-neuron integration of zebrafish ascending and descending dopaminergic systems. *Nat. Commun.* **2**, 171 (2011).
8. Dunn, T. W. *et al.* Brain-wide mapping of neural activity controlling zebrafish exploratory locomotion. *Elife* **5**, e12741 (2016).
9. Wolf, S. *et al.* Sensorimotor computation underlying phototaxis in zebrafish. *Nat. Commun.* **8**, 651 (2017).
10. Kimmel, C. B., Ballard, W. W., Kimmel, S. R., Ullmann, B. & Schilling, T. F. Stages of embryonic development of the zebrafish. *Dev. Dyn.* **203**, 253–310 (1995).
11. Portavella, M., Vargas, J. ., Torres, B. & Salas, C. The effects of telencephalic pallial lesions on spatial, temporal, and emotional learning in goldfish. *Brain Res. Bull.* **57**, 397–399 (2002).
12. Fogueira, M. *et al.* Morphogenesis underlying the development of the everted teleost telencephalon. *Neural Dev.* **7**, 32 (2012).
13. Blankenship, A. G. & Feller, M. B. Mechanisms underlying spontaneous patterned

- activity in developing neural circuits. *Nat. Rev. Neurosci.* **11**, 18–29 (2010).
14. Tsodyks, M. Linking Spontaneous Activity of Single Cortical Neurons and the Underlying Functional Architecture. *Science (80-.)*. **286**, 1943–1946 (1999).
 15. Fernández Galán, R. & Galán, R. F. On how network architecture determines the dominant patterns of spontaneous neural activity. *PLoS One* **3**, e2148 (2008).
 16. Takahashi, N., Sasaki, T., Matsumoto, W., Matsuki, N. & Ikegaya, Y. Circuit topology for synchronizing neurons in spontaneously active networks. *Proc. Natl. Acad. Sci. U. S. A.* **107**, 10244–9 (2010).
 17. Viventi, J. *et al.* Flexible, foldable, actively multiplexed, high-density electrode array for mapping brain activity in vivo. *Nat. Neurosci.* **14**, 1599–605 (2011).
 18. Portugues, R., Severi, K. E., Wyart, C. & Ahrens, M. B. Optogenetics in a transparent animal: circuit function in the larval zebrafish. *Curr. Opin. Neurobiol.* **23**, 119–126 (2013).
 19. Ramdya, P., Reiter, B. & Engert, F. Reverse correlation of rapid calcium signals in the zebrafish optic tectum in vivo. *J. Neurosci. Methods* **157**, 230–7 (2006).
 20. Portugues, R., Feierstein, C. E., Engert, F. & Orger, M. B. Whole-Brain Activity Maps Reveal Stereotyped, Distributed Networks for Visuomotor Behavior. *Neuron* **81**, 1328–1343 (2014).
 21. Mukamel, E. A., Nimmerjahn, A. & Schnitzer, M. J. Automated analysis of cellular signals from large-scale calcium imaging data. *Neuron* **63**, 747–60 (2009).
 22. Churchland, M. M. *et al.* Neural population dynamics during reaching. *Nature* **487**, 51–6 (2012).
 23. Ben-Ari, Y., Gaiarsa, J.-L., Tyzio, R. & Khazipov, R. GABA: a pioneer transmitter that excites immature neurons and generates primitive oscillations. *Physiol. Rev.* **87**, 1215–84 (2007).
 24. Leinekugel, X., Khalilov, I., Ben-Ari, Y. & Khazipov, R. Giant depolarizing potentials: the septal pole of the hippocampus paces the activity of the developing intact septohippocampal complex in vitro. *J. Neurosci.* **18**, 6349–57 (1998).
 25. Namiki, S. *et al.* Layer III neurons control synchronized waves in the immature

- cerebral cortex. *J. Neurosci.* **33**, 987–1001 (2013).
26. Leinekugel, X. Correlated Bursts of Activity in the Neonatal Hippocampus in Vivo. *Science (80-.)*. **296**, 2049–2052 (2002).
 27. Ahrens, M. B., Orger, M. B., Robson, D. N., Li, J. M. & Keller, P. J. Whole-brain functional imaging at cellular resolution using light-sheet microscopy. *Nat. Methods* **10**, 413–20 (2013).
 28. Heusser, A. C., Poeppel, D., Ezzyat, Y. & Davachi, L. Episodic sequence memory is supported by a theta?gamma phase code. *Nat. Neurosci.* **19**, 1374–1380 (2016).
 29. Wikenheiser, A. M. & Redish, A. D. Hippocampal theta sequences reflect current goals. *Nat. Neurosci.* **18**, 289–294 (2015).
 30. Paulsen, O. & Sejnowski, T. J. Natural patterns of activity and long-term synaptic plasticity. *Curr. Opin. Neurobiol.* **10**, 172–9 (2000).
 31. Whishaw, I. Q. & Vanderwolf, C. H. Hippocampal EEG and behavior: changes in amplitude and frequency of RSA (theta rhythm) associated with spontaneous and learned movement patterns in rats and cats. *Behav. Biol.* **8**, 461–84 (1973).
 32. Watts, D. J. & Strogatz, S. H. Collective dynamics of ‘small-world’ networks. *Nature* **393**, 440–2 (1998).
 33. Saint-Amant, L. & Drapeau, P. Motoneuron Activity Patterns Related to the Earliest Behavior of the Zebrafish Embryo. *J. Neurosci.* **20**, 3964–3972 (2000).
 34. Muto, A. *et al.* Genetic visualization with an improved GCaMP calcium indicator reveals spatiotemporal activation of the spinal motor neurons in zebrafish. *Proc. Natl. Acad. Sci. U. S. A.* **108**, 5425–30 (2011).
 35. Warp, E. *et al.* Emergence of patterned activity in the developing zebrafish spinal cord. *Curr. Biol.* **22**, 93–102 (2012).
 36. Kiehn, O. Development and functional organization of spinal locomotor circuits. *Curr. Opin. Neurobiol.* **21**, 100–109 (2011).
 37. Ljunggren, E. E., Haupt, S., Ausborn, J., Ampatzis, K. & El Manira, A. Optogenetic activation of excitatory premotor interneurons is sufficient to generate coordinated locomotor activity in larval zebrafish. *J. Neurosci.* **34**, 134–9 (2014).

38. Mueller, T., Vernier, P. & Wullimann, M. F. A phylotypic stage in vertebrate brain development: GABA cell patterns in zebrafish compared with mouse. *J. Comp. Neurol.* **494**, 620–634 (2006).
39. Moly, P. K., Ikenaga, T., Kamihagi, C., Islam, A. F. M. T. & Hatta, K. Identification of initially appearing glycine-immunoreactive neurons in the embryonic zebrafish brain. *Dev. Neurobiol.* **74**, 616–632 (2014).
40. Randlett, O. *et al.* Whole-brain activity mapping onto a zebrafish brain atlas. *Nat. Methods* **12**, 1039–1046 (2015).
41. Wu, Y.-J. *et al.* Unilateral stimulation of the lateral division of the dorsal telencephalon induces synaptic plasticity in the bilateral medial division of zebrafish. *Sci. Rep.* **7**, 9096 (2017).
42. Friston, K., Phillips, J., Chawla, D. & Büchel, C. Nonlinear PCA: characterizing interactions between modes of brain activity. *Philos. Trans. R. Soc. Lond. B. Biol. Sci.* **355**, 135–46 (2000).
43. Wilson, R. E. Binary-star light curve models. *Publ. Astron. Soc. Pacific* **106**, 921 (1994).
44. Alivisatos, A. P. *et al.* The brain activity map project and the challenge of functional connectomics. *Neuron* **74**, 970–4 (2012).
45. Allen, W. E. *et al.* Global Representations of Goal-Directed Behavior in Distinct Cell Types of Mouse Neocortex. *Neuron* **94**, 891–907.e6 (2017).
46. Ziv, Y. *et al.* Long-term dynamics of CA1 hippocampal place codes. *Nat. Neurosci.* **16**, 264–266 (2013).
47. Liberti, W. A. *et al.* Unstable neurons underlie a stable learned behavior. *Nat. Neurosci.* (2016). doi:10.1038/nn.4405
48. Engert, F. Neuron NeuroView The Big Data Problem: Turning Maps into Knowledge. *Neuron* **83**, 1246–1248 (2014).
49. Wolf, S. *et al.* Whole-brain functional imaging with two-photon light-sheet microscopy. *Nat. Methods* **12**, 379–380 (2015).
50. Hildebrand, D. G. C. *et al.* Whole-brain serial-section electron microscopy in larval

- zebrafish. *Nature* **545**, 345–349 (2017).
51. Guzowski, J. F. *et al.* Mapping behaviorally relevant neural circuits with immediate-early gene expression. *Current Opinion in Neurobiology* **15**, 599–606 (2005).
 52. Mirich, J. M., Illig, K. R. & Brunjes, P. C. Experience-dependent activation of extracellular signal-related kinase (ERK) in the olfactory bulb. *J. Comp. Neurol.* **479**, 234–241 (2004).
 53. Hussain, A. *et al.* High-affinity olfactory receptor for the death-associated odor cadaverine. *Proc. Natl. Acad. Sci. U. S. A.* **110**, 19579–84 (2013).
 54. Briggman, K. L. & Bock, D. D. Volume electron microscopy for neuronal circuit reconstruction. *Current Opinion in Neurobiology* **22**, 154–161 (2012).
 55. Kasthuri, N. *et al.* Saturated Reconstruction of a Volume of Neocortex. *Cell* **162**, 648–661 (2015).
 56. Kreshuk, A., Koethe, U., Pax, E., Bock, D. D. & Hamprecht, F. A. Automated Detection of Synapses in Serial Section Transmission Electron Microscopy Image Stacks. *PLoS One* **9**, e87351 (2014).
 57. Jurrus, E. *et al.* Detection of neuron membranes in electron microscopy images using a serial neural network architecture. *Med. Image Anal.* **14**, 770–783 (2010).
 58. Lichtman, J. W., Pfister, H. & Shavit, N. The big data challenges of connectomics. *Nat. Neurosci.* **17**, 1448–54 (2014).
 59. Yan, G. *et al.* Network control principles predict neuron function in the *Caenorhabditis elegans* connectome. *Nature* (2017). doi:10.1038/nature24056
 60. Rubinov, M. & Sporns, O. Complex network measures of brain connectivity: uses and interpretations. *Neuroimage* **52**, 1059–69 (2010).
 61. Reimann, M. W. *et al.* Cliques of Neurons Bound into Cavities Provide a Missing Link between Structure and Function. *Front. Comput. Neurosci.* **11**, 48 (2017).
 62. Tan, L. & Jiang, J. Novel adaptive IIR filter for frequency estimation and tracking [DSP Tips&Tricks. *IEEE Signal Process. Mag.* **26**, 186–189 (2009).
 63. Blumhagen, F. *et al.* Neuronal filtering of multiplexed odour representations. *Nature* **479**, 493–498 (2011).

64. Pietri, T. *et al.* The Emergence of the Spatial Structure of Tectal Spontaneous Activity Is Independent of Visual Inputs. *Cell Rep.* **19**, 939–948 (2017).
65. Palmér, T. *et al.* Action sequencing in the spontaneous swimming behavior of zebrafish larvae - implications for drug development. *Sci. Rep.* **7**, 3191 (2017).
66. Mizuseki, K. & Buzsáki, G. Preconfigured, Skewed Distribution of Firing Rates in the Hippocampus and Entorhinal Cortex. *Cell Rep.* **4**, 1010–1021 (2013).
67. Buzsáki, G. & Mizuseki, K. The log-dynamic brain: how skewed distributions affect network operations. *Nat. Rev. Neurosci.* **15**, 264–78 (2014).
68. Ronneberger, O. *et al.* ViBE-Z: a framework for 3D virtual colocalization analysis in zebrafish larval brains. *Nat. Methods* **9**, 735–742 (2012).
69. Takahashi, M., Inoue, M., Tanimoto, M., Kohashi, T. & Oda, Y. Short-term desensitization of fast escape behavior associated with suppression of Mauthner cell activity in larval zebrafish. *Neurosci. Res.* (2017). doi:10.1016/j.neures.2017.03.008
70. Asakawa, K. *et al.* Genetic dissection of neural circuits by Tol2 transposon-mediated Gal4 gene and enhancer trapping in zebrafish. *Proc. Natl. Acad. Sci. U. S. A.* **105**, 1255–60 (2008).
71. Breakspear, M., Heitmann, S. & Daffertshofer, A. Generative models of cortical oscillations: neurobiological implications of the kuramoto model. *Front. Hum. Neurosci.* **4**, 190 (2010).
72. Hansel, D., Mato, G. & Meunier, C. Clustering and slow switching in globally coupled phase oscillators. *Phys. Rev. E* **48**, 3470–3477 (1993).
73. Rosen, M. J. A Theoretical Neural Integrator. *IEEE Trans. Biomed. Eng.* **BME-19**, 362–367 (1972).
74. Loewenstein, Y. & Sompolinsky, H. Temporal integration by calcium dynamics in a model neuron. *Nat. Neurosci.* **6**, 961–967 (2003).
75. Hutcheon, B. *et al.* Resonance, oscillation and the intrinsic frequency preferences of neurons. *Trends Neurosci.* **23**, 216–22 (2000).
76. Torrence, C. & Compo, G. P. A Practical Guide to Wavelet Analysis. *Bull. Am. Meteorol. Soc.* **79**, 61–78 (1998).

77. Quian Quiroga, R., Kraskov, A., Kreuz, T. & Grassberger, P. Performance of different synchronization measures in real data: A case study on electroencephalographic signals. *Phys. Rev. E* **65**, 41903 (2002).
78. Vinck, M., van Wingerden, M., Womelsdorf, T., Fries, P. & Pennartz, C. M. A. The pairwise phase consistency: a bias-free measure of rhythmic neuronal synchronization. *Neuroimage* **51**, 112–22 (2010).
79. Hurtado, J. M., Rubchinsky, L. L. & Sigvardt, K. A. Statistical method for detection of phase-locking episodes in neural oscillations. *J. Neurophysiol.* **91**, 1883–98 (2004).
80. Dugué, L., Marque, P. & VanRullen, R. The phase of ongoing oscillations mediates the causal relation between brain excitation and visual perception. *J. Neurosci.* **31**, 11889–93 (2011).
81. Neuling, T., Rach, S., Wagner, S., Wolters, C. H. & Herrmann, C. S. Good vibrations: Oscillatory phase shapes perception. *Neuroimage* **63**, 771–778 (2012).
82. Prez-Schuster, V. *et al.* Sustained Rhythmic Brain Activity Underlies Visual Motion Perception in Zebrafish. *Cell Rep.* **17**, 1098–1112 (2016).
83. Sumbre, G., Muto, A., Baier, H. & Poo, M. Entrained rhythmic activities of neuronal ensembles as perceptual memory of time interval. *Nature* **456**, 102–6 (2008).
84. Cheng, R.-K., Jesuthasan, S. J. & Penney, T. B. Zebrafish forebrain and temporal conditioning. *Philos. Trans. R. Soc. London B Biol. Sci.* **369**, (2014).
85. Ahrens, M. B. *et al.* Brain-wide neuronal dynamics during motor adaptation in zebrafish. *Nature* **485**, 471–7 (2012).
86. Tabor, R., Yaksi, E. & Friedrich, R. W. Multiple functions of GABA A and GABA B receptors during pattern processing in the zebrafish olfactory bulb. *Eur. J. Neurosci.* **28**, 117–27 (2008).
87. Kleiner, M. *et al.* What’s new in Psychtoolbox-3? *Perception* **36**, S14 (2007).
88. Chen, T.-W. *et al.* Ultrasensitive fluorescent proteins for imaging neuronal activity. *Nature* **499**, 295–300 (2013).
89. Miri, A., Daie, K., Burdine, R. D., Aksay, E. & Tank, D. W. Regression-based identification of behavior-encoding neurons during large-scale optical imaging of

- neural activity at cellular resolution. *J. Neurophysiol.* **105**, 964–80 (2011).
90. Berens, P. **CircStat**: A *MATLAB* Toolbox for Circular Statistics. *J. Stat. Softw.* **31**, (2009).
 91. Gonçalves, P. J., Arrenberg, A. B., Hablitzel, B., Baier, H. & Machens, C. K. Optogenetic perturbations reveal the dynamics of an oculomotor integrator. *Front. Neural Circuits* **8**, 10 (2014).
 92. Miri, A. *et al.* Spatial gradients and multidimensional dynamics in a neural integrator circuit. *Nat. Neurosci.* **14**, 1150–9 (2011).
 93. Kastnerhuber, E., Kratochwil, C. F., Ryu, S., Schweitzer, J. & Driever, W. Genetic dissection of dopaminergic and noradrenergic contributions to catecholaminergic tracts in early larval zebrafish. *J. Comp. Neurol.* **518**, 439–458 (2010).
 94. Easter, S. S. & Nicola, G. N. The development of vision in the zebrafish (*Danio rerio*). *Dev. Biol.* **180**, 646–63 (1996).
 95. Muto, A., Ohkura, M., Abe, G., Nakai, J. & Kawakami, K. Real-time visualization of neuronal activity during perception. *Curr. Biol.* **23**, 307–11 (2013).
 96. Orger, M. B. *et al.* Behavioral screening assays in zebrafish. *Methods Cell Biol.* **77**, 53–68 (2004).
 97. Portugues, R., Haesemeyer, M., Blum, M. L. & Engert, F. Whole-field visual motion drives swimming in larval zebrafish via a stochastic process. *J. Exp. Biol.* **218**, 1433–43 (2015).
 98. Valente, A., Huang, K.-H., Portugues, R. & Engert, F. Ontogeny of classical and operant learning behaviors in zebrafish. *Learn. Mem.* **19**, 170–7 (2012).
 99. Best, J. D. *et al.* Non-associative learning in larval zebrafish. *Neuropsychopharmacology* **33**, 1206–15 (2008).
 100. Harvey, C. D., Coen, P. & Tank, D. W. Choice-specific sequences in parietal cortex during a virtual-navigation decision task. *Nature* **484**, 62–8 (2012).
 101. Trivedi, C. A. & Bollmann, J. H. Visually driven chaining of elementary swim patterns into a goal-directed motor sequence: a virtual reality study of zebrafish prey capture. *Front. Neural Circuits* **7**, 86 (2013).

102. Ahrens, M. B., Huang, K. H., Narayan, S., Mensh, B. D. & Engert, F. Two-photon calcium imaging during fictive navigation in virtual environments. *Front. Neural Circuits* **7**, 104 (2013).
103. Braida, D. *et al.* Role of neuronal nicotinic acetylcholine receptors (nAChRs) on learning and memory in zebrafish. *Psychopharmacology (Berl)*. **231**, 1975–85 (2014).
104. Jouary, A., Haudrechy, M., Candelier, R. & Sumbre, G. A 2D virtual reality system for visual goal-driven navigation in zebrafish larvae. *Sci. Rep.* **6**, 34015 (2016).
105. Kirkpatrick, S., Gelatt, C. D. & Vecchi, M. P. Optimization by Simulated Annealing. *Science (80-.)*. **220**, 671–680 (1983).
106. Vargas, J. P., Bingman, V. P., Portavella, M. & López, J. C. Telencephalon and geometric space in goldfish. *Eur. J. Neurosci.* **24**, 2870–8 (2006).